

Impaired Myofibroblast Proliferation is a Central Feature of Pathologic Post-Natal Alveolar Simplification

Imran S. Khan^{1,2}, Christopher Molina^{2,3,4}, Xin Ren^{2,3,4}, Vincent C. Auyeung^{2,3,4}, Max Cohen^{3,4}, Tatsuya Tsukui^{2,3,4}, Amha Atakilit^{2,3,4}, Dean Sheppard^{2,3,4,*}

¹Division of Neonatology, Department of Pediatrics, UCSF

²Cardiovascular Research Institute, UCSF

³Division of Pulmonary, Critical Care, Allergy, and Sleep, UCSF

⁴Department of Medicine, UCSF

*Address correspondence to:

Dean Sheppard
University of California, San Francisco
PO BOX 589001, ROOM 252R
San Francisco, CA 94158-9001
E-mail: Dean.Sheppard@ucsf.edu

Abbreviations:

α -SMA, alpha-smooth muscle actin; BPD, bronchopulmonary dysplasia; cHet, conditional heterozygous; cKO, conditional knockout; EdU, 5-ethynyl-2'-deoxyuridine; PDGFR α , platelet-derived growth factor receptor alpha; P, postnatal day; scRNA-seq, single-cell RNA-sequencing; TGF β , transforming growth factor-beta; TGF β R2, transforming growth factor-beta receptor 2; UMAP, Uniform Manifold Approximation and Projection.

Abstract

Premature infants with bronchopulmonary dysplasia (BPD) have impaired alveolar gas exchange due to alveolar simplification and dysmorphic pulmonary vasculature. Advances in clinical care have improved survival for infants with BPD, but the overall incidence of BPD remains unchanged because we lack specific therapies to prevent this disease. Recent work has suggested a role for increased transforming growth factor-beta (TGF β) signaling and myofibroblast populations in BPD pathogenesis, but the functional significance of each remains unclear. Here, we utilize multiple murine models of alveolar simplification and comparative single-cell RNA sequencing to identify shared mechanisms that could contribute to BPD pathogenesis. Single-cell RNA sequencing reveals a profound loss of myofibroblasts in two models of BPD and identifies gene expression signatures of increased TGF β signaling, cell cycle arrest, and impaired proliferation in myofibroblasts. Using pharmacologic and genetic approaches, we find no evidence that increased TGF β signaling in the lung mesenchyme contributes to alveolar simplification. In contrast, this is likely a failed compensatory response, since none of our approaches to inhibit TGF β signaling protect mice from alveolar simplification due to hyperoxia while several make simplification worse. In contrast, we find that impaired myofibroblast proliferation is a central feature in several murine models of BPD, and we show that inhibiting myofibroblast proliferation is sufficient to cause pathologic alveolar simplification. Our results underscore the importance of impaired myofibroblast proliferation as a central feature of alveolar simplification and suggest that efforts to reverse this process could have therapeutic value in BPD.

Introduction

During the alveolar phase of lung development, alveolar walls protrude from secondary crests into the lumen of existing airways and form new alveoli to increase the lung's surface area for gas exchange ¹.

Many premature infants are born prior to the onset of alveogenesis and develop bronchopulmonary dysplasia (BPD), a chronic lung disease of prematurity caused by developmental arrest of secondary alveolar septation². Over 50 years ago, Northway and colleagues described BPD as a heterogeneous pattern of severe lung injury with pathologic findings of severe inflammation, airway dysplasia, and fibrosis³. Despite advances in neonatal care, the incidence of BPD remains unchanged as 30% of infants born before 30 weeks of gestation will develop BPD^{2,4}. More infants are now surviving at earlier gestational ages, and the lungs of these infants have a “new” BPD phenotype characterized by a homogenous process of alveolar simplification, dysmorphic pulmonary vasculature, and mild airway thickening and fibrosis^{1,2}. BPD is defined clinically by the need for prolonged respiratory support and supplemental oxygen, and infants with BPD suffer from long-term morbidity including severe respiratory infections, reactive airway disease, pulmonary hypertension, and neurodevelopmental impairment^{1,2}.

The inflammatory response plays a significant role in BPD pathogenesis and results from a combination of perinatal infection, oxygen toxicity, and barotrauma from mechanical ventilation¹. Several recent studies have suggested a role for the pro-fibrotic cytokine transforming growth factor-beta (TGF β) in BPD pathogenesis⁴⁻⁹. Infants with BPD have increased TGF β in serum and bronchoalveolar lavage fluid¹⁰⁻¹³. Experimentally, murine models of BPD show increased TGF β signaling and activation of downstream fibrotic pathways^{7-9,14-17}. At the same time, TGF β plays an important role in normal development, and complete loss of TGF β signaling impairs either embryonic lung development or alveolar septation¹⁸⁻²⁹. TGF β is a known regulator of myofibroblasts in fibrotic disease³⁰, but it also drives mesenchymal cells to commit towards the myofibroblast lineage during embryonic lung development²¹. Despite its essential role in normal lung development, the functional significance of increased TGF β signaling in BPD pathogenesis remains unclear.

Alveolar myofibroblasts are contractile mesenchymal cells that are critical for alveolar septation³¹. They are characterized by the expression of platelet-derived growth factor receptor alpha (PDGFR α), alpha-smooth muscle actin (α -SMA), and the production of elastin^{21,31-34}. Myofibroblasts are derived from PDGFR α + mesenchymal cells at birth and peak during alveogenesis when they colocalize with secondary septae^{21,31,33-35}. Ablation of PDGFR α + cells in neonatal mice causes alveolar simplification, while neonatal hyperoxia treatment causes loss of PDGFR α + fibroblasts, dysregulated alveolar elastin deposition, and impaired PDGFR α + cell contractility^{31,33,34,36}. Inhibition of myofibroblast contraction has been shown to lead to alveolar simplification³⁷. These studies support a fundamental functional role for myofibroblasts during alveogenesis, but whether the number of myofibroblasts is reduced in BPD or experimental models of BPD remains controversial^{31,34,38-40}.

To identify conserved mechanism of injury in BPD pathogenesis, we implemented a novel strategy to compare two murine models of alveolar simplification by single-cell RNA-sequencing (scRNA-seq): neonatal hyperoxia exposure and loss of epithelial TGF β signaling. Using flow cytometry and sequencing, we observed a dramatic reduction of myofibroblasts in both models of disease. Additionally, we found that increased TGF β signaling, decreased PDGFR α signaling, and impaired proliferation are hallmark features of injured myofibroblasts during alveogenesis. Blocking TGF β through several different approaches consistently worsened hyperoxia-induced disease, suggesting TGF β plays an essential homeostatic function in both normal alveolar development and hyperoxia-induced disease, but that increased TGF β signaling does not seem to be an important driver of alveolar simplification. We also demonstrated that PDGFR α + cells undergo robust proliferation during normal alveogenesis, but this proliferation is impaired in both hyperoxia-treated and TGF β -manipulated mice. We showed that modulation of PDGFR α + cell proliferation is sufficient to cause alveolar simplification, even in the absence of inflammation or hyperoxic injury. These studies demonstrate that PDGFR α +

cells are profoundly sensitive to injury during alveogenesis, they require TGF β signaling, and their proliferation is essential for normal alveolar development.

Results

Neonatal Hyperoxia Exposure and Loss of Epithelial TGF β Signaling Both Cause Alveolar Simplification.

To identify conserved features of lung injury in bronchopulmonary dysplasia (BPD), we compared two different mouse models of lung injury known to cause alveolar simplification in mice. We first implemented the hyperoxia-induced model of BPD in which newborn mice are exposed to 75% oxygen from postnatal day (P) 0-10 and then recovered in room air until analysis (Figure 1A). This model takes advantage of the fact that mice are born during the saccular phase of lung development and undergo alveolarization from postnatal day P4 – P39⁴¹⁻⁴³. We harvested lungs to analyze alveolar architecture after completion of alveolarization at P40. Hyperoxia-treated mice showed significant alveolar airspace enlargement compared to controls (Figure 1B). Consistent with findings from other groups using similar protocols^{31,34}, we did not see evidence of fibrosis, scarring or inflammation. In parallel, we used the flexiVent rodent ventilator to measure respiratory mechanics. Hyperoxia-treated mice had increased total lung capacity, increased compliance, and decreased elastance compared to control mice (Figure 1C). These findings are consistent with those of emphysematous lungs, and these physiologic changes align with the enlarged, simplified alveolar structures observed by histology⁴⁴⁻⁴⁶.

For our second model of alveolar simplification, we generated mice which lack the critical TGF β receptor TGFBR2 in lung epithelium by crossing Nkx2.1-cre to the *Tgfb2* conditional allele (*Tgfb2*^{F/F};Nkx2.1-cre). These mice are viable at birth, have no respiratory distress, gain normal weight, and generate expected ratios of offspring with respect to each genotype (data not shown). Lungs from

conditional knockout (cKO) mice show enlarged airspaces consistent with alveolar simplification, confirming earlier reports that TGF β signaling in lung epithelium is required for normal secondary septation (Figure 1D-E)²⁶. We then used the flexiVent system to analyze respiratory mechanics in cKO mice and observed increased compliance and decreased elastance comparable to what we saw in hyperoxia-exposed mice (Figure 1F). Previous work demonstrated that *Tgfb2*^{F/F};Nkx2.1-cre mice are protected from lung disease caused by transgenic overexpression of TGF β 1 or neonatal hyperoxia treatment²⁶. To our surprise, *Tgfb2*^{F/F};Nkx2.1-cre mice were not protected from disease in our model of neonatal hyperoxia, but rather developed worse disease. These data suggest TGF β signaling to the lung epithelium is required for both normal alveologenesis and that it plays a protective role in the response to hyperoxia-induced injury.

Profound Loss of PDGFR α + Fibroblasts During Hyperoxia Treatment.

To begin exploring the mechanisms underlying alveolar simplification in these models, we treated wildtype mice with hyperoxia from P0-P10 and analyzed dissociated lung cells by flow cytometry at P10. While we observed changes in many cell types of the lung with hyperoxia treatment, the most striking result was the profound loss of PDGFR α + fibroblasts (Figure 2A-B). Using flow cytometry, we found that both the percentage and absolute number of PDGFR α + fibroblasts were substantially reduced with hyperoxia treatment (Figure 2B). Next, we analyzed *Tgfb2*^{F/F};Nkx2.1-cre mice at P10 in normoxia and observed a similar phenotype of reduced PDGFR α + fibroblasts (Figure 2C-D). While the magnitude of reduction was less impressive than we observed in the hyperoxia model, the most significant change in cell numbers in *Tgfb2*^{F/F};Nkx2.1-cre mice was the reduction in PDGFR α + fibroblasts. Together, these results are consistent with earlier studies which showed a loss of PDGFR α + cells with neonatal hyperoxia treatment and reinforce the critical role of PDGFR α + fibroblasts in normal alveolar development^{31,36}.

scRNA-seq Reveals Loss of Myofibroblasts in Both Models of Alveolar Simplification.

To identify conserved molecular and cellular mechanisms underlying pathologic alveolar simplification, we performed single-cell RNA sequencing on lungs from *Tgfbr2*^{F/F} (CTRL) and *Tgfbr2*^{F/F}; *Nkx2.1-cre* (cKO) mice in either normoxia or hyperoxia (Figure 3A). This approach allowed for simultaneous comparison of both injury models: normoxia versus hyperoxia in CTRL mice, and CTRL versus cKO mice in normoxia (Figure 3B). Given the reduction of PDGFR α + fibroblasts observed by flow cytometry in both models of lung injury, we hypothesized that changes in the lung mesenchyme might play a substantial role in the pathogenesis of alveolar simplification. To ensure sufficient mesenchymal cells in our analysis, we used flow cytometric sorting to enrich for mesenchymal and epithelial cells by limiting the input of hematopoietic and endothelial cells. After processing and combining all samples, we identified 24 clusters from 26,610 cells (Figure S1A-C). We focused our analysis on the lung mesenchyme and assigned identities to 7 distinct clusters by referencing previously published scRNA-seq studies of the developing lung (Figures 3C and S1D)⁴⁷⁻⁵⁰.

Although flow cytometry had already shown a profound loss of PDGFR α + cells in these two injury models, we could not attribute this loss to a specific fibroblast subset. Our single cell data enabled higher resolution assessment of the dynamics of fibroblast subsets (Figure 3D). In particular, we observed a significant loss of alveolar and ductal myofibroblast clusters in both models of injury (Figure 3D-E), suggesting that the reduction of PDGFR α + cells by flow cytometry was due to the loss of alveolar and ductal myofibroblasts. To externally validate these findings, we re-analyzed two recently published scRNA-seq studies in which mice were treated with 85% oxygen from P0-P14^{47,50}. Consistent with our own data, hyperoxia-treated mice in both studies showed a significant loss of myofibroblasts within the lung mesenchyme (Figure S2).

To gain insight into the molecular mechanisms driving the loss of myofibroblasts, we used Qiagen Ingenuity Pathway Analysis (IPA) to compare differential gene expression in the myofibroblasts in both models of injury ⁵¹. After filtering for upregulated pathways, we identified 32 predicted upstream regulators that were shared in both models (Figure 3F). Of these pathways, we noted several predictions corresponding to TGF β signaling, inhibitors of cell cycle, and Wnt signaling. These results are notable because TGF β is a known driver of myofibroblast differentiation and profibrotic programs in fibroblasts ^{21,30}, while its overall contribution to alveolar simplification and BPD is unclear ^{5,52}. The prediction of increased cell cycle inhibition is also of interest because it suggests that the reduction of myofibroblasts in these models might be caused by their impaired proliferation.

We used the NicheNet software package to gain insight into the specific cell-cell interactions which might be impacting the myofibroblasts in these two models of lung injury ⁵³. We reasoned that epithelial-myofibroblast signals would be particularly important, since the defect in the cKO model is restricted to epithelial cells, yet the most prominent phenotype is found in myofibroblasts. To explore this further, we used NicheNet to identify shared patterns of changes in ligand-receptor signaling originating from the lung epithelium to the myofibroblasts (Figure 4A). Here we again noted an increase in TGF β signaling to the myofibroblasts (Figure 4B). Of the decreased pathways, the most notable were Pdgfa-Pdgfra and Shh-Hhip, both of which are known to be critical for myofibroblast differentiation and function (Figure 4C) ^{29,54}. Additionally, the predicted reduction of Pdgfra signaling aligns with our flow cytometry data showing a loss of PDGFR α + fibroblasts in both injury models as well as a reduction in the mean fluorescence intensity of PDGFR α antibody staining in these cells (Figure 2B-D). Together, these data suggest that epithelial dysfunction may cause myofibroblast defects through loss of supportive signals and gain of inhibitory signals.

TGF β Signaling Plays Homeostatic Role in Normal Alveolar Development and in Hyperoxia.

Both IPA and NicheNet analyses predicted that TGF β signaling is activated in myofibroblasts in both models of alveolar simplification (Figures 3 and 4). Given the conflicting literature regarding the role of TGF β in normal lung development^{5,18,52}, we sought to determine the functional significance of TGF β signaling during postnatal alveologenesis in both normoxic and hyperoxic conditions. We hypothesized that if excessive TGF β signaling is a pathologic response in hyperoxia, titration of a pan-TGF β -blocking antibody (1D11) could identify a therapeutic window to protect from disease while permitting normal development under normoxic conditions. Alternatively, worsened disease with 1D11 treatment would suggest that increased TGF β is a compensatory response to injury rather than a primary driver of disease in the hyperoxia model. To test these hypotheses, we injected wildtype mice with 0, 10, 20 or 30 mg/kg of 1D11 from P2-P10 in either normoxia or hyperoxia and then harvested at P40 for analysis by histology (Figure 5A). To our surprise, we found that while only the highest dose of 1D11 treatment caused alveolar simplification in normoxia, all doses of 1D11 treatment caused worse alveolar simplification in hyperoxia compared to PBS (Figure 5B). Consistent with these histology results, lung physiology studies of 1D11-treated mice showed a pattern of emphysematous changes with increased compliance and decreased elastance (Figure 5C). These changes are similar to what we previously observed in hyperoxia-treated mice and in *Tgfb2^{F/F};Nkx2.1-cre* mice and complement the histologic findings of alveolar simplification in 1D11-treated mice. Together, these results support the alternative hypothesis that TGF β signaling plays a homeostatic role in both normal alveolar development and in hyperoxia.

Because 1D11 antibody treatment is systemic, we were unable to attribute the results of these studies to a specific cell type within the lung. Our current study, consistent with earlier reports, demonstrates that TGF β signaling to the epithelium is required for normal alveolar development as well as an adaptive response to hyperoxia²⁶. To interrogate the role of TGF β signaling to the lung mesenchyme, we sought to cross *Tgfb2^{F/F}* mice to either the *Pdgfra^{CreER}* or *Gli1^{CreER}* allele to target *Tgfb2* in

myofibroblasts and mesenchymal cells during alveogenesis. While *Pdgfra*^{CreER} has been used to specifically target PDGFR α + cells⁵⁵, many studies have also used the broader *Gli1*^{CreER} to target myofibroblasts during alveolar lung development^{29,54}. Because the *Pdgfra*^{CreER} and *Gli1*^{CreER} alleles were generated using a knock-in/knock-out approach, mice carrying the CreER allele are haploinsufficient for *Pdgfra* or *Gli1*, respectively^{55,56}. We conducted hyperoxia studies in each of these two lines and found that the *Gli1*^{CreER} allele alone does not disrupt alveolar development in either normoxia or with hyperoxia treatment (Figure S3A-B). In contrast, mice with the *Pdgfra*^{CreER} allele undergo normal development in normoxia, but they develop worse alveolar simplification with hyperoxia treatment compared to their cre-negative littermates (Figure S3A-B). These data support use of the *Gli1*^{CreER} allele to target the lung mesenchyme in either normoxia or hyperoxia while limiting the use of *Pdgfra*^{CreER} mice (and other *Pdgfra*-haploinsufficient alleles) to normoxic conditions.

Based on these validation studies, we generated *Tgfbr2*^{F/F}; *Gli1*^{CreER/+} mice to study the effects of TGF β signaling to the lung mesenchyme. Interestingly, we observed a similar pattern of lung disease as 1D11 treatment when deleting *Tgfbr2* in the lung mesenchyme: *Tgfbr2*^{F/F}; *Gli1*^{CreER/+} mice developed alveolar simplification in normoxia when compared to littermate controls, and they developed worse disease than their littermates with hyperoxia exposure (Figure S4A-B). Together, these results show that TGF β signaling is required to both the lung epithelium and mesenchyme for normal development, that it plays a homeostatic role in response to neonatal hyperoxia treatment, and that all our efforts to inhibit TGF β made hyperoxia-induced alveolar simplification worse.

To address mechanisms of TGF β activation in normal alveolar development and in the hyperoxia model of alveolar simplification, we generated *Itgb6*^{F/F} mice and crossed them to the Nkx2.1-cre allele. The α v β 6 integrin is expressed predominantly in epithelial tissues, activates TGF β *in vivo*, and has been shown to be a critical mediator of lung injury in models of acute lung injury and pulmonary fibrosis⁵⁷⁻⁶².

Itgb6^{F/F};Nkx2.1-cre mice lack $\alpha v\beta 6$ on lung epithelial cells and undergo normal alveolar development, but to our surprise, show no difference in disease severity with hyperoxia treatment (Figure S4C-D). Within the mesenchyme, $\alpha v\beta 1$ and $\alpha v\beta 8$ have been shown to activate TGF β *in vivo*⁶²⁻⁶⁵, so we next deleted all αv -integrins in the lung mesenchyme by crossing *Itgav*^{F/F} mice to the *Gli1*^{CreER} allele. These mice develop spontaneous alveolar simplification in normoxic conditions, have lung physiology parameters consistent with an emphysematous phenotype, and develop worse lung disease with hyperoxia exposure (Figure 6A-C). These data suggest that $\alpha v\beta 6$ does not play a role in TGF β activation during normal development or neonatal hyperoxia, while αv -integrins in the lung mesenchyme are required for normal development and play a protective role in response to hyperoxia.

Impaired Proliferation of PDGFR α + Fibroblasts with Hyperoxia Treatment.

Flow cytometry and scRNA-seq both showed a reduction of PDGFR α + fibroblasts in hyperoxia-treated mice, which suggests these cells are exquisitely sensitive to injury. To address whether this might be due to impaired proliferation as suggested by IPA analysis, we exposed wildtype mice to hyperoxia and treated them with the nucleoside analogue 5-ethynyl-2'-deoxyuridine (EdU) to identify proliferating cells. We found a decrease of PDGFR α + cells in hyperoxia-treated mice by P8 both by percentage and by absolute number (Figure 7A-C), which persisted to P10 and continued even with 4 days of normoxic recovery. Using EdU analysis, we found hyperoxia caused a proliferative defect in PDGFR α + cells as early as P4, preceding the decrease in cell number. This early impairment of proliferation by PDGFR α + cells was the most striking change observed across all subsets in our EdU analysis, and suggests that a proliferative defect contributes to the decreased cell number.

After observing impaired proliferation of PDGFR α + cells in the hyperoxia model of lung injury, we explored whether this mechanism is conserved across our other models of alveolar simplification. We used EdU treatment and flow cytometry to characterize cell subsets and proliferation in

$\text{Tgfb2}^{\text{F/F}}$; Nkx2.1-cre mice and 1D11-treated wildtype mice. Remarkably, both models showed a similar reduction of PDGFR α + cells along with decreased PDGFR α + cell proliferation as quantified by EdU uptake (Figure 8A-D). These results provide functional validation of our IPA analyses showing enrichment of cell cycle inhibitory pathways in injured myofibroblasts, and they suggest impaired PDGFR α + cell proliferation might be a conserved feature of developmental lung injuries which result in alveolar simplification.

Impaired Proliferation of PDGFR α + Fibroblasts Is Sufficient to Cause Alveolar Simplification.

After observing impaired PDGFR α + cell proliferation in multiple models of alveolar simplification, we sought to determine whether inhibiting proliferation in these cells would be sufficient to cause disease. We generated mice with conditional deletion of *Ect2*, a protein required for cytokinesis⁶⁶, by crossing the $\text{Ect2}^{\text{F/F}}$ mice with the $\text{Pdgfra}^{\text{CreER}}$ allele. We found earlier that PDGFR α + cells underwent robust proliferation through P10 in normoxic conditions (Figure 7C), so we analyzed $\text{Ect2}^{\text{F/F}};\text{Pdgfra}^{\text{CreER/+}}$ mice at P14 to characterize the impact of this mouse model on the cellular composition of the lung during early alveogenesis. Using flow cytometry, we observed a significant reduction in PDGFR α + cells within the lung by percentage and absolute number (Figure 9A-B). While this reduction in PDGFR α + cells was expected in $\text{Ect2}^{\text{F/F}};\text{Pdgfra}^{\text{CreER/+}}$ mice, it was interesting that *Pdgfra* expression was reduced in the remaining PDGFR α + cells as quantified by mean fluorescence intensity (MFI). Earlier studies found a correlation between *Pdgfra* expression levels and fibroblast proliferation⁶⁷, so we wondered whether this phenotype of reduced *Pdgfra* expression was conserved across the other injury models in this study which showed reduced PDGFR α + cell proliferation. Indeed, quantification of PDGFR α MFI by flow cytometry confirmed that *Pdgfra* expression is significantly reduced in the lung mesenchyme and specifically in PDGFR α + cells in each of the injury models we analyzed in this study (Figure S5A).

Next, we aged $\text{Ect2}^{\text{FF}};\text{Pdgfra}^{\text{CreER}+/+}$ mice until P40 to analyze their lungs by either morphometry or lung physiology. By histology, we observed enlarged alveolar airspaces and increased MLI's in conditional knockouts ($\text{Ect2}^{\text{FF}};\text{Pdgfra}^{\text{CreER}+/+}$) compared to controls (Figure 7C). Importantly, conditional heterozygous mice showed no difference in MLI compared to cre-negative mice, which confirms that haploinsufficiency of *Pdgfra* caused by using the $\text{Pdgfra}^{\text{CreER}}$ allele in normoxic conditions is not responsible for this phenotype (Figures 7C and S5A-B). By lung physiology, $\text{Ect2}^{\text{FF}};\text{Pdgfra}^{\text{CreER}+/+}$ mice produced the same emphysematous phenotype of increased compliance and decreased elastance which we observed in several other models of alveolar simplification in this study (Figure 7D). Together, these data demonstrate that impaired proliferation of PDGFR α + cells is sufficient to cause alveolar simplification, even in the absence of environmental insult or modulation of TGF β signaling.

Discussion

Using a combination of flow cytometry, lung physiology, and scRNA-seq, we identified several core features of lung injury that are conserved across multiple mouse models of alveolar simplification. We first compared neonatal hyperoxia exposure (75% hyperoxia P0-P10) to the loss of epithelial TGF β signaling ($\text{Tgfbr2}^{\text{FF}};\text{Nkx2.1-cre}$). Flow cytometric analysis of both models showed a significant reduction of PDGFR α + cells, while scRNA-seq studies attributed these changes to a loss of alveolar and ductal myofibroblasts. Qiagen IPA and NicheNet ligand-receptor analyses identified several pathways that were upregulated in injured myofibroblasts in both models: increased TGF β signaling, enrichment of inhibitors of cell cycle, and decreased Pdgfa-Pdgfra signaling. Using a combination of pharmacologic and genetic approaches, we demonstrated that increased TGF β signaling in the mesenchyme does not seem to be a driver of alveolar simplification, but rather that TGF β signaling is critical for both normal alveolar development and for protecting against impaired alveolar development in response to hyperoxia. In contrast, we show that PDGFR α + cell proliferation is reduced in multiple models of

alveolar simplification, and that this impaired proliferation on its own is sufficient to cause alveolar simplification.

Several recent studies have identified lung mesenchymal cells as critical mediators of alveologenesis. Li *et al.* established the requirement of myofibroblasts during postnatal development by specifically ablating PDGFR α + cells at the onset of alveologenesis and showing that these mice developed alveolar simplification³¹. Other work has identified essential functions of myofibroblasts during alveolar development, including contractility³⁷ and mitochondrial energetics⁶⁸. Ricetti *et al* used bulk RNA sequencing to show a skewing from myofibroblast to matrix fibroblast phenotypes after hyperoxia exposure along with reduced Ki-67 uptake and contractility in myofibroblasts³⁶. Our current study builds on this existing body of work by characterizing significant changes in PDGFR α + cell number in several models of developmental lung injury. By flow cytometry, we found reduction in the number of PDGFR α + cells in hyperoxia-treated mice and in Tgfbr2^{F/F};Nkx2.1-cre mice during the early phase of alveologenesis. Using scRNA-seq, we attributed this reduction to the alveolar and ductal myofibroblast populations. Importantly, we identified myofibroblast proliferation as a critical feature of normal alveolar development and validated this observation in several experimental models.

NicheNet analysis of our scRNA-seq data predicted decreased Pdgfa-Pdgfra signaling from the epithelium to the myofibroblasts in both hyperoxia-treated and Tgfbr2^{F/F};Nkx2.1-cre mice. This observation is interesting because several studies have focused on the requirement of Pdgfa-Pdgfra interactions for myofibroblast identity and function. Deletion of *Pdgfra* in mesenchymal populations of the neonatal lung has been shown to disrupt alveologenesis^{54,69}. Other studies have found lower *Pdgfra* expression in lung samples from BPD patients^{40,70}. In our current study we use flow cytometry to show a loss of PDGFR α + cells in multiple models of alveolar simplification: hyperoxia-treated mice, Tgfbr2^{F/F};Nkx2.1-cre mice, 1D11-treated mice, and Ect2^{F/F};Pdgfra^{CreER/+} mice. In addition to the loss of

PDGFR α + cells, we also observed decreased *Pdgfra* expression within the remaining PDGFR α + cells (Figure S5A). Given that EdU uptake is also reduced amongst the remaining PDGFR α + cells these results suggest Pdgfa-Pdgfra signaling might regulate myofibroblast proliferation in addition to their identity and function during neonatal lung development.

As part of our current studies, we conducted control experiments with the *Gli1*^{CreER} and *Pdgfra*^{CreER} alleles and discovered results with broad implications for others utilizing similar genetic tools for their work. Both alleles were generated using a knock-in/knock-out gene targeting approach which disrupts the native expression of *Gli1* and *Pdgfra*, respectively^{55,56}. Because Hedgehog and Pdgfa-Pdgfra signaling pathways are important for lung development^{71,72}, we sought to validate the effects of haploinsufficiency of *Gli1* and *Pdgfra* when using these alleles. Both *Gli1*^{CreER/+} and *Pdgfra*^{CreER/+} mice underwent normal alveolar development in normoxic conditions when compared to cre-negative littermates. In contrast, *Pdgfra*^{CreER/+} mice developed worse alveolar simplification after hyperoxia treatment compared to their cre-negative littermates (*Pdgfra*^{+/+}). The *Gli1*^{CreER} results suggest this allele can be used for conditional knockout studies in either normoxic or hyperoxic conditions with little impact from *Gli1* haploinsufficiency. The *Pdgfra*^{CreER} results, however, should serve as a caution to researchers utilizing genetic tools with *Pdgfra*-haploinsufficiency.

Recent work has established an essential role for TGF β signaling in normal alveolar development⁵², but the functional role of TGF β in models of BPD and alveolar simplification remains unclear. Our scRNA-seq data showed increased TGF β signaling in myofibroblasts in two injury models, so we hypothesized that excess TGF β signaling might be a driver of disease pathogenesis. To determine the functional significance of TGF β in the hyperoxia model, we treated mice with the pan-TGF β -blocking antibody 1D11. Because TGF β is required for normal alveologenesis, we hypothesized a dose titration approach might identify a “sweet spot” to neutralize an excess of TGF β in hyperoxia while preserving

normal development in normoxia. Instead, we found that every dose of 1D11 treatment worsened hyperoxia-induced alveolar simplification while only the highest dose caused disease in normoxia. While the 1D11-normoxia results confirm an essential role for TGF β in normal alveolar development, the 1D11-hyperoxia results suggest TGF β plays a homeostatic function rather than a pathologic role in the hyperoxia model of injury. Because 1D11 treatment neutralizes TGF β ligands systemically, we used Nkx2.1-cre and Gli1^{CreER/+} alleles to conditionally delete *Tgfb2* in the lung epithelium and mesenchyme, respectively. Confirming earlier reports, we found that disrupting TGF β signaling to either of these populations causes alveolar simplification^{26,29}. Of significance, however, both Tgfb2^{F/F};Nkx2.1-cre and Tgfb2^{F/F};Gli1^{CreER/+} mice developed worse disease with neonatal hyperoxia treatment. Taken together with our 1D11-hyperoxia experiments, we conclude that TGF β signaling to both the lung epithelium and mesenchyme is required for normal alveolar development and is protective rather than pathologic in hyperoxia-perturbed alveolar development.

Little is known about mechanisms of TGF β activation in alveolar development and neonatal lung injury. TGF β ligands are secreted as latent, inactive complexes that are anchored to the cell surface or the extracellular matrix⁶². These complexes prevent TGF β from engaging its receptors, and therefore TGF β activation is tightly regulated in tissues despite the high levels of latent TGF β complex⁶². Integrins are cell-surface proteins that regulate interactions in the extracellular matrix, and several studies by our group have demonstrated that the epithelial integrin α v β 6 is critical for TGF β activation in models of acute lung injury and pulmonary fibrosis^{58,60,73,74}. However, TGF β activation by α v β 6 does not play a role in alveolar development in either normoxia or hyperoxia. We then deleted α v-integrins in the lung mesenchyme since α v β 1 and α v β 8 are the only other integrins known to activate TGF β *in vivo*⁶². Interestingly, deletion of α v-integrins under normoxic conditions only produced a modest degree of alveolar simplification but clearly led to more severe alveolar simplification after hyperoxia.

We originally hypothesized that increased TGF β signaling was a pathologic response to neonatal hyperoxia treatment and that targeting the TGF β pathway might protect from disease pathogenesis. While our results disproved this hypothesis, they also seem at odds with published data where blocking TGF β signaling was beneficial in various lung injury models. For example, it was unexpected that *Tgfb2^{F/F};Nkx2.1-cre* mice develop worse lung injury in our hyperoxia-induced model of BPD because earlier work showed these same mice to be protected from hyperoxia²⁶. We suspect this difference in outcome can be explained by the more aggressive models of lung injury used by this earlier study. Specifically, these authors used either transgenic overexpression of TGF β or 100% hyperoxia exposure which both resulted in neonatal mortality and severe inflammation, neither of which are observed in our model of 75% hyperoxia. Additionally, many earlier studies focused on TGF β activation in hyperoxia-induced BPD utilized chronic 85% hyperoxia such as P0-P14 or P0-P28, both of which result in inflammation and fibrosis^{8,14-16,75}. Similarly, one earlier study used transgenic expression of IL-1 β in the developing airways to produce a BPD-like phenotype due to inflammation⁷⁶. Deletion of *Itgb6*, and therefore loss of epithelial α v β 6 integrins, conferred partial protection from disease in this injury model⁶¹. A common theme across these earlier studies implicating TGF β in pathology is that they utilized aggressive models of lung injury which caused severe inflammation, fibrosis, and neonatal mortality, all of which recapitulate the histopathologic features of “old BPD” in the clinical setting. In contrast, the hyperoxia model used in our current study more closely represents the “new BPD” phenotype of emphysematous changes with simplified alveolar structures in the absence of lung scarring and fibrosis^{1,2}. Collectively, these data suggests that while inhibition of TGF β may have some protective role in severe injury models associated with significant fibrosis, the major functions of TGF β signaling during normal alveolar development and in response to moderate hyperoxia are homeostatic and protective.

There are several limitations to our current study. We used flow cytometry to phenotype population-level changes across several models of neonatal lung injury. While flow cytometry is a powerful tool to

quantify population subsets and sort cells for scRNA-seq, it requires tissue digestion and generation of single-cell suspensions for downstream analysis. The cells which survive these protocols may represent a skewed population and may not be completely representative of *in vivo* conditions. For example, many fragile and dying/apoptotic cells do not survive this processing and would be excluded from analysis. Another drawback to flow cytometry is that our ability to define population subsets is limited by the knowledge and feasibility of using cell-surface markers to faithfully distinguish cell types within each population. Recent work by our group has identified cell-surface markers to characterize fibroblast subsets in the adult lung by flow cytometry, but we are unaware of similar protocols to address fibroblast heterogeneity in the neonatal lung⁷⁷. We used scRNA-seq to characterize cell subsets within the lung mesenchyme, but the identification and validation of cell-surface proteins suitable for flow cytometric analysis of these same populations is beyond the scope of this current study. Our scRNA-seq data, together with emerging scRNA-seq from multiple other laboratories should provide a rich dataset for others to identify cell surface markers that allow more precise analysis and sorting of distinct mesenchymal populations in the developing lung.

In summary, our current work highlights the essential role of myofibroblast proliferation and TGF β signaling in normal alveologenesis. We show that myofibroblasts are depleted during neonatal lung injury and that their loss is at least partially due to impaired proliferation and expansion during this critical window of development. We confirm the results of others in the field who have observed increased TGF β signatures in the hyperoxia-injured neonatal lung that generated hope for targeting this pathway as a therapeutic intervention for BPD. However, after conducting exhaustive studies targeting TGF β ligands, receptors and activating integrins, we conclude that increased TGF β signaling in myofibroblasts more likely represents a failed compensatory mechanism rather than a central driver of disease pathogenesis. Finally, our sequencing data should provide useful insights to the broader community studying alveolar development and neonatal lung injury. Although our current work focuses

on a few of the genes and pathways highlighted by these data, we are optimistic that others will utilize this dataset to expand our understanding of the molecular mechanisms driving both normal and aberrant alveolar development.

Figure Legend

Figure 1. Neonatal Hyperoxia Treatment and Loss of Epithelial TGF β Signaling Both Cause Alveolar Simplification.

(A) Wildtype C57BL/6 mice were treated in 75% hyperoxia versus normoxia from P0-P10 and recovered in room air until harvest at P40 for analysis by either histology or lung physiology. **(B)** H&E sections of representative lungs from (A) harvested at P40 (left) with quantification of mean linear intercept (right). **(C)** Mice treated as in (A) and harvested for lung physiology measurements of compliance, elastance and lung capacity. **(D)** $Tgfb2^{F/F}$ and $Tgfb2^{F/F};Nkx2.1\text{-cre}$ littermates were treated in hyperoxia versus normoxia from P0-P10 and recovered in room air until harvest at P40 for analysis by histology. **(E)** H&E sections of representative lungs from (D) harvested at P40 (left) with quantification of mean linear intercept (right). **(F)** Normoxia cohort treated as in (D) and harvested for lung physiology measurements of compliance, elastance and lung capacity. Data in (B), (C), and (F) compared by 2-tailed unpaired Student's t-test. Data in (E) compared by ANOVA with Fisher's post hoc test. Error bars depict mean \pm SEM. ** $p<0.01$, *** $p<0.001$, **** $p<0.0001$. Scale bars = 100 μm .

Figure 2. Loss of PDGFR α + Cells With Neonatal Hyperoxia Treatment and Loss of Epithelial TGF β Signaling.

(A) Wildtype C57BL/6 mice were treated in 75% hyperoxia versus normoxia from P0-P10 and harvested on P10 for analysis by flow cytometry. Graph on right shows total cells per left lung as quantified by flow cytometry. **(B)** Representative flow cytometry plots of the lung mesenchyme (live, CD45-, CD31-, and Epcam-) with gates depicting PDGFR α + cells (left). Major cell populations of the lung were defined by the indicated cell surface markers and shown as either a percentage of all cells (top) or as absolute number (bottom). **(C)** $Tgfb2^{F/F}$ and $Tgfb2^{F/F};Nkx2.1\text{-cre}$ littermates were maintained in normoxic conditions from P0-P10 and harvested on P10 for analysis by flow cytometry. Graph on right shows total cells per left lung as quantified by flow cytometry. **(D)** Flow cytometry plots for (C)

using the same gating strategy as described above. Data in (A-D) analyzed by 2-tailed unpaired Student's t-test. Error bars depict mean \pm SEM. *p<0.05, **p<0.01, ***p<0.001, ****p<0.0001.

Figure 3. scRNA-seq Reveals Loss of Myofibroblasts in Both Models of Alveolar Simplification.

(A) Schematic of scRNA-seq project showing CTRL ($Tgfb2^{F/F}$) and cKO ($Tgfb2^{F/F};Nkx2.1-cre$) littermates treated in 75% hyperoxia versus normoxia from P0-P10 and harvested on P7 or P14 for FACS-purification and analysis by scRNA-seq. n=2 mice harvested for each genotype, treatment condition and timepoint. **(B)** Venn-diagram depicting strategy to compare these two models to identify shared features of alveolar simplification. **(C)** UMAP projection of mesenchymal cells from scRNA-seq as outlined in (A). **(D)** Bar graphs depicting the frequency of each cell type by treatment condition, genotype, and timepoint. **(E)** The frequency of alveolar and ductal myofibroblasts within the mesenchyme as depicted in (D) with each data point representing either a biologic or technical replicate. Because the data depicts both biologic and technical replicates, no statistics were performed on this data set. **(F)** Differentially expressed genes in myofibroblasts were identified by comparing either CTRL RA vs O2 cells or RA CTRL vs cKO cells. These lists were subsequently analyzed by Qiagen IPA to identify predicted upstream regulators for each comparison. The Venn-diagram on left depicts the number of overlapping predicted upstream regulators with z-score >1.5 (upregulated), while the table on right lists these 32 shared upstream regulators. Blue = TGF β signaling, red = inhibitors of cell cycle, green = Wnt signaling.

Figure 4. NicheNet Ligand-Receptor Analysis of Epithelial-Mesenchymal Crosstalk in Both Models of Alveolar Simplification. scRNA-seq data was analyzed using the NicheNet software package. **(A)** Alveolar epithelial clusters were pooled to define sender population and myofibroblast clusters were pooled to define receiver population. By analyzing differential expression of ligands, receptors, and downstream gene expression changes in myofibroblasts, NicheNet predicted increased (left) or decreased (right) ligand-receptor signaling in each comparison of interest. Gray boxes show

ligands expressed on the epithelium and the purple-shaded boxes indicate the corresponding receptors expressed on myofibroblasts. Upper panels compare hyperoxia versus normoxia in CTRL cells. Lower panels compare CTRL versus cKO cells in normoxia. **(B)** List of ligand-receptor pairs predicted to be increased in both injury models. *Tgfb1-Tgfb2* pairings highlighted in blue. **(C)** List of ligand-receptor pairs predicted to be decreased in both injury models. *Pdgfa-Pdgfra* and *Pdgfb-Pdgfrb* pairings highlighted in red.

Figure 5. Inhibiting TGF β Disrupts Alveolar Development and Exacerbates Hyperoxia-induced Injury. **(A)** Wildtype C57BL/6 mice were injected every other day from P2-P10 with PBS or 1D11 (pan-TGF β -blocking antibody), treated in 75% hyperoxia treatment versus normoxia from P0-P10, and recovered in room air until harvest at P40 for analysis by either histology or lung physiology. **(B)** H&E sections of representative lungs from (A) harvested at P40 (left). Images shown are from PBS and 30 mg/kg 1D11 treatment groups. Mean linear intercepts calculated for all treatment groups (right). **(C)** PBS- and 30 mg/kg 1D11-treated mice treated in normoxic conditions as in (A) and harvested for lung physiology measurements of compliance, elastance and lung capacity at P40. Data in (B) compared by ANOVA with Fisher's post hoc test; for readability and limitations of graphing, only the statistical significance values within normoxia or hyperoxia cohorts are plotted. Data in (C) compared by 2-tailed unpaired Student's t-test. Error bars depict mean \pm SEM. *p<0.05, **p<0.01, ****p<0.0001. Scale bars = 100 μ m.

Figure 6. Deletion of αv -integrins in Lung Mesenchyme Impairs Alveolar Development and Worsens Hyperoxia-induced Injury. **(A)** *Itgav*^{F/F} and *Itgav*^{F/F}; *Gli1*^{CreER/+} littermates were injected with tamoxifen on P2 and P4, treated in 75% hyperoxia versus normoxia from P0-P10, and recovered in room air until harvest at P40 for analysis by either histology or lung physiology. **(B)** H&E sections of representative lungs from (A) harvested at P40 (left). Mean linear intercepts calculated for all treatment

groups (right). **(C)** Normoxia cohort treated as in (A) and harvested for lung physiology measurements of compliance, elastance and lung capacity. Data in (B) compared by ANOVA with Fisher's post hoc test. Data in (C) compared by 2-tailed unpaired Student's t-test. Error bars depict mean \pm SEM.

*p<0.05, **p<0.01, ****p<0.0001. Scale bars = 100 μ m.

Figure 7. Impaired Proliferation of PDGFR α + Fibroblasts With Neonatal Hyperoxia Treatment. (A) Wildtype C57BL/6 mice were treated in 75% hyperoxia versus normoxia from P0-P10 and recovered in room air until indicated timepoints for analysis. Mice were injected with EdU 24 hours prior to each analysis timepoint. **(B)** Flow cytometry plots of lung mesenchyme (CD45-, CD31-, Epcam-, MCAM-) show gating of PDGFR α + cells (upper panels) and subsequent identification of EdU+/PDGFR α + cells (lower panels). Panels on far-right show an EdU-untreated littermate used to define EdU+ gate. **(C)** Time course graphs showing indicated populations of the lung as percent of lung (top), total cells in left lung (middle), and percent EdU+ cells (bottom). Data graphed as mean \pm with exception of EdU+ panel in which each animal is plotted individually. Data compared by 2-tailed unpaired Student's t-test.

*p<0.05, **p<0.01, ***p<0.001, ****p<0.0001.

Figure 8. Impaired PDGFR α + Cell Proliferation is a Conserved Feature Across Multiple Models of Alveolar Simplification. (A) Tgfb2 $^{F/F}$ and Tgfbr2 $^{F/F}$;Nkx2.1-cre littermates were maintained in normoxic conditions from P0-P7, injected with EdU on P6, and harvested 24 hours later on P7 for flow cytometry. **(B)** Flow cytometry plots of lung mesenchyme (CD45-, CD31-, Epcam-, MCAM-) show gating of PDGFR α + cells (left panels) and subsequent identification of EdU+/PDGFR α + cells (right panels). Graphs on far right show major cell populations of the lung by percentage (upper graphs) and percent EdU-positive within each of these populations (lower graphs). **(C)** Wildtype C57BL/6 mice were injected every other day from P2-P8 with PBS or 30 mg/kg 1D11 (pan-TGF β -blocking antibody) in normoxic conditions, injected with EdU on P9, and harvested 24 hours later on P10 for flow cytometry.

(D) Flow cytometry plots of lung mesenchyme (CD45-, CD31-, Epcam-, MCAM-) show gating of PDGFR α + cells (left panels) and subsequent identification of EdU+/PDGFR α + cells (right panels). Graphs on far right show major cell populations of the lung by percentage (upper graphs) and percent EdU-positive within each of these populations (lower graphs). Data in analyzed by 2-tailed unpaired Student's t-test. Error bars depict mean \pm SEM. *p<0.05, **p<0.01, ***p<0.001, ****p<0.0001.

Figure 9. Blocking Proliferation of PDGFR α + Fibroblasts is Sufficient to Cause Alveolar Simplification. (A) Ect2^{F/F} and Ect2^{F/F};Pdgfra^{CreER/+} littermates were injected with tamoxifen on P2 and P4 in normoxic conditions. Mice were analyzed by flow cytometry on P14 or aged until P40 for analysis by either histology or lung physiology. **(B)** Representative flow cytometry plots of the lung mesenchyme (live, CD45-, CD31-, and Epcam-) with gates depicting PDGFR α + cells (left). Major cell populations of the lung were defined by the indicated cell surface markers and shown as either a percentage of all cells (top) or as absolute number (bottom). **(C)** H&E sections of representative lungs from (A) harvested at P40 (left). Mean linear intercepts calculated for all treatment groups (right). **(D)** Mice treated as in (A) and harvested for lung physiology measurements of compliance, elastance and lung capacity. Data in (B) compared by 2-tailed unpaired Student's t-test. Data in (C) compared by ANOVA with Fisher's post hoc test. Error bars depict mean \pm SEM. **p<0.01, ***p<0.001, ****p<0.0001. Scale bars = 100 μ m.

Supplementary Figure Legend

Supplementary Figure 1. scRNA-seq of Murine Lungs With Neonatal Hyperoxia Treatment or Loss of Epithelial TGF β Signaling. (A) UMAP projection of all scRNA-seq data. (B) UMAP plots showing expression levels of canonical markers for epithelial, endothelial, hematopoietic, mesenchymal, and mesothelial populations. (C) Total cell number within each of the indicated major lung populations. (D) Dot plot showing representative markers for each cluster within the mesenchyme. (E) Differentially expressed genes in myofibroblasts were identified by comparing either CTRL RA vs O2 cells or RA CTRL vs cKO cells. These lists were subsequently analyzed by Qiagen IPA to identify predicted upstream regulators for each comparison. The Venn-diagram on left depicts the number of overlapping predicted upstream regulators with z-score <-1.5 (upregulated), while the table on right lists these 40 shared upstream regulators.

Supplementary Figure 2. Re-analysis of Published Data Confirms Loss of Myofibroblasts With Neonatal Hyperoxia Treatment. (A) Hurskainen *et al.* treated C57BL/6 wildtype mice with 85% hyperoxia versus normoxia from P0-P14 and analyzed the lungs by scRNA-seq at P3, P7, and P14⁴⁷. The Seurat object used for publication was provided by the authors. UMAP projection shows the mesenchymal populations as defined by Hurskainen *et al.* (B) By using metadata within the Seurat object, we graphed the frequency of each mesenchymal population by treatment condition and time point. (C) The frequency of myofibroblasts within the mesenchyme as depicted in (B). (D) Xia *et al.* treated C57BL/6 wildtype mice with 85% hyperoxia versus normoxia from P0-P14 and analyzed the lungs by scRNA-seq at P14⁵⁰. The Seurat object used for publication was provided by the authors. UMAP projection shows the mesenchymal populations as defined by Xia *et al.* (E) By using metadata within the Seurat object, we graphed the frequency of each mesenchymal population by treatment condition and time point. (F) The frequency of alveolar and ductal myofibroblasts within the

mesenchyme as depicted in (E). Graphs in (C) and (F) depict one value for each condition because we were unable to extract replicate values from the data provided.

Supplementary Figure 3. $\text{Gli1}^{\text{CreER}}$ Allele Does Not Disrupt Alveolar Development, But $\text{Pdgfra}^{\text{CreER}}$ Allele Worsens Hyperoxia-induced Injury. (A) Either $\text{Gli1}^{\text{CreER}/+}$ or $\text{Pdgfra}^{\text{CreER}/+}$ mice and their cre-negative littermates were injected with tamoxifen on P2 and P4, treated in 75% hyperoxia versus normoxia from P0-P10, and recovered in room air until harvest at P40 for analysis by histology. (B) Mean linear intercepts of $\text{Gli1}^{\text{CreER}/+}$ and $\text{Gli1}^{+/+}$ mice treated as outlined in (A) and harvested at P40. (C) Mean linear intercepts of $\text{Pdgfra}^{\text{CreER}/+}$ and $\text{Pdgfra}^{+/+}$ mice treated as outlined in (A) and harvested at P40. Data compared by ANOVA with Fisher's post hoc test. Error bars depict mean \pm SEM. ***p<0.001, ****p<0.0001.

Supplementary Figure 4. Loss of TGF β Signaling to Lung Mesenchyme Causes Worse Disease in Hyperoxia While Itgb6 Plays No Role in Alveolar Development. (A) $\text{Tgfbr2}^{\text{F/F}}$ and $\text{Tgfbr2}^{\text{F/F}};\text{Gli1}^{\text{CreER}/+}$ littermates were injected with tamoxifen on P2 and P4, treated in 75% hyperoxia versus normoxia from P0-P10, and recovered in room air until harvest at P40 for analysis by histology. (B) H&E sections of representative lungs from (A) harvested at P40 (left). Mean linear intercepts calculated for all treatment groups (right). (C) $\text{Itgb6}^{\text{F/F}}$ and $\text{Itgb6}^{\text{F/F}};\text{Nkx2.1-cre}$ littermates were treated in 75% hyperoxia versus normoxia from P0-P10, and recovered in room air until harvest at P40 for analysis by histology (D) H&E sections of representative lungs from (C) harvested at P40 (left). Mean linear intercepts calculated for all treatment groups (right). Data compared by ANOVA with Fisher's post hoc test. Error bars depict mean \pm SEM. *p<0.05, ***p<0.001, ****p<0.0001. Scale bars = 100 μm .

Supplementary Figure 5. Decreased PDGFR α Mean Fluorescence Intensity Across Multiple Models of Alveolar Simplification. (A) Mean fluorescence intensity (geometric mean, MFI) of

PDGFR α antibody staining on MCAM-negative mesenchymal cells (CD45-, CD31-, Epcam-) and PDGFR α + cells (CD45-, CD31-, Epcam-, MCAM-, PDGFR α +) as quantified by flow cytometry. Each column represents an experiment shown earlier in this study: normoxia vs hyperoxia at P10 (Figure 2), Tgfbr2^{F/F} vs Tgfbr2^{F/F};Nkx2.1-cre at P10 (Figure 2), PBS vs 1D11 at P10 (Figure 8), Ect2^{F/F} vs Ect2^{F/F};Pdgfra^{CreER/+} at P14 (Figure 9). To compare values across multiple experiments, MFI's were normalized to the control condition within each experiment. Data compared by ANOVA with Fisher's post hoc test. Error bars depict mean \pm SEM. ***p<0.001, ****p<0.0001.

Materials and Methods

Mice

C57BL/6 (Stock No. 000664), Nkx2.1-cre (Stock No. 008661), Pdgfra^{CreER} (Stock No. 032770), and Gli1^{CreER} (Stock No. 007913), and Itgav^{F/F} (Stock No. 032297) mouse lines were obtained from the Jackson Laboratory. Tgfb2^{F/F} mice (exon 2 conditional allele) were described previously⁷⁸. Ect2^{F/F} were described previously⁶⁶, and were obtained from Dr. Alan Fields at Mayo Clinic. All lines were maintained on the C57BL/6 genetic background except for the Ect2^{F/F} line, which was originally generated in BALB/c and backcrossed 5 generations to C57BL/6 for these studies. All animal experiments were in accordance with protocols approved by the Institutional Animal Care and Use Committee and Laboratory Animal Resource Center.

Neonatal Hyperoxia Treatment

The hyperoxia animal chamber (BioSpherix) was attached to a medical oxygen source controlled by a ProOx single gas controller (BioSpherix) set to maintain 75% oxygen under normobaric conditions. Birth was defined as <12 hours of life, and pups assigned to hyperoxia were transferred into the chamber with lactating dams and maintained from P0-P10 and then recovered in normoxia. During hyperoxia treatment, lactating dams were rotated between hyperoxia and normoxia to prevent maternal injury and to control for nutrition amongst both cohorts. Mice in both conditions were given nestlets and trail mix for additional enrichment. Mice in both conditions remained under typical 7a-7p light cycling, and chamber was checked daily to monitor temperature, humidity, and gas controller function.

Tamoxifen, Antibody, and EdU Treatments

Tamoxifen (Sigma) was dissolved in corn oil (Sigma) at 15 mg/ml, and 150 µg (10 µl) was administered via intraperitoneal (i.p.) injections on P2 and P4. Antibody clone 1D11 was used for pan-TGF β -blocking

studies ⁷⁹, and was generated in our laboratory from a hybridoma obtained from ATCC. Antibody was diluted in PBS and administered via i.p. injections at 0, 10, 20 or 30 mg/kg on P2, P4, P6, P8 and P10. For proliferation studies, EdU (Thermo Fisher) was reconstituted in DMSO at 100 mg/ml, diluted in PBS to 5 mg/ml, and injected i.p. at 75 mg/kg 24 hours prior to harvest.

Generation of *Itgb6* Flox Mice

Itgb6 flox mice (*Itgb6*^{F/F}) were made by CRISPR/Cas9-aided homology-directed repair. Loxp sequences were inserted to flank exon 4 of *Itgb6*. Two guide RNA target sequences were chosen in the introns upstream and downstream of exon 4. crRNAs were obtained from IDT with input sequences CAGCTTATCATCCATCTAAA (upstream) and ACCTTCCTCTGACGCACCTT (downstream). Two 200bp donor DNAs were obtained from IDT. EcoRV sites (gatatc) were inserted following loxp sequences for screening purposes. The sequences of the donor DNAs are as follows:

Upstream donor DNA:

TAATCTCTCCTTATTTGGCTCACCTTCTGCAACCACACACCAAGAAAGGGCAGCTTATCATCCA
TCTAAAATACTTCGTATAGCATACATTATACGAAGTTATgatatcTGGATGCTACTTCTCCCTAGGAG
ATATAAAATATCCAACATACACACCTCCTCTGCCTCAATCCTCAC

Downstream donor DNA:

TAACCTACATTTTTCTCTGAGTTTCTATCAAATAACAATTTCACCTCCTCTGACGCAC
TTATAACTTCGTATAGCATACATTATACGAAGTTATgatatcGGGAAATGTGGCTTCACTCATTGCTG
AGAGCAGCAGCCTTCATTGCAATTAAAGTCAAGAGGAAATGGG.

CRISPR/Cas9 complex (Cas9, crRNA, trRNA) and donor DNA were injected into C57BL/6 fertilized zygotes, which were then implanted into the oviducts of pseudopregnant female mice. 28 pups were born, and 6 of them had at least one allele with desired loxp insertion with two of them being homozygous for recombinant alleles. We picked one founder to expand the colony. Genotyping was performed with a forward primer 5'- CTGCAACCACACACCAAGAA-3' and a reverse primer 5'-

GCCTGACCTTATTAAGCTGCA-3', which provide 196bp bands for wild type alleles and 236bp bands for flox alleles.

Histology

For morphometry studies, lungs were inflated with ice-cold 4% paraformaldehyde (PFA) under constant pressure of 25 cm H₂O for 5 minutes. Lungs were carefully dissected of attached structures and transferred into vial containing cold 4% PFA. Samples were rocked in 4°C overnight, washed 3x with PBS, and dehydrated in a series of ethanol (30%, 50% and 70%). Tissues were submitted in 70% ethanol to the UCSF Gladstone Histology and Light Microscopy core for further processing for paraffin embedding and tissue blocks were sectioned for Hematoxylin and Eosin (H&E) staining. For quantification of mean linear intercept (MLI), 6-8 sections of 5 μ m thickness were sampled at 20 μ m levels through each set of lungs. Images were acquired on a Nikon Ti Inverted Microscope using a 10x objective and DS-Ri2 color camera. For each sample, approximately 30 images were acquired from which 12 were randomly selected for MLI quantification using ImageJ software as described previously⁸⁰. All samples were blinded during imaging and MLI quantification.

Lung Physiology

Pulmonary compliance and elastance were analyzed using the flexiVent system (SCIREQ) as previously described⁴⁵. Mice were anesthetized with ketamine (100 mg/kg), xylazine (10 mg/kg), and acepromazine (3 mg/kg) before a tracheostomy was performed to cannulate the trachea with a 20-gauge catheter. Mice were then paralyzed with pancuronium (0.1 mg/kg) and analyzed using the flexiVent rodent ventilator. All mice were analyzed in a blinded fashion.

Tissue Dissociation

Mouse lungs were harvested after perfusion through the right ventricle with PBS. Lungs were dissected into individual lobes, minced with razor blades, and suspended in protease solution [0.25 % Collagenase A (Millipore Sigma), 1 U/ml Dispase II (Millipore Sigma), 2000 U/ml Dnase I (Millipore Sigma) in Dulbecco's Modified Eagle Medium (Thermo Fisher) containing 10 mM HEPES (Millipore Sigma) and 2% FBS (Millipore Sigma)]. The suspension was incubated in a 37°C water bath in a 15 ml conical for 25 minutes with aggressive trituration by glass Pasteur pipette every 8 minutes. The digestion was then quenched for 5 minutes in ice-cold PBS containing 5% FBS and 2 mM EDTA before passing cells through a 70 µm cell strainer. Cells were pelleted and resuspended in Red Blood Cell Lysing Buffer HybriMax (Sigma) for 5 minutes. RBC lysis was quenched dropwise with 5% FBS/PBS and cells were passed through a 40 µm cell strainer, washed, and resuspended in 5% FBS/PBS containing antibodies for FACS purification.

Flow Cytometry and Fluorescence-activated Cell Sorting (FACS)

After tissue dissociation, cells were resuspended in 5% FBS/PBS with Fc-blocking antibody (TruStain FcX; BioLegend) at 0.01 mg/ml for 5 minutes at room temperature. All antibodies were resuspended in Brilliant Stain Buffer (BD Biosciences) and added to Fc-blocked cells for final antibody concentration of 1:200. Cells were stained for 30 minutes on ice for surface antibody staining, washed, and then passed through another 40 µm before analysis and/or cell sorting. DRAQ7 (BioLegend) was used 1:1000 to identify dead cells. Flow cytometric cell counting was performed using CountBright Plus Absolute Counting Beads (Thermo Fisher). The following antibodies were used in this study: anti-CD9 (clone MZ3, PE; BioLegend), anti-CD31 (clone 390, A488, BV605; BioLegend, BD Biosciences), anti-CD45 (clone 30F-11, BV786, APC/Cy7, PE/Cy7; BioLegend, BD Biosciences), anti-Epcam (clone G8.8, FITC, PE, PE/Cy7; BioLegend), anti-I-A/I-E (clone M5/114.15.2, APC/Cy7, Spark UV 387; BioLegend), anti-Mcam (clone ME-9F1, A488, BUV496; BioLegend, BD Biosciences), anti-Pdgfra (clone APA5, APC, BV421, PE/Cy7; BioLegend). For proliferation studies, cells were stained for surface markers as described above and then washed, fixed, permeabilized, and processed for Click-iT EdU detection

according to manufacturer's protocol (Click-iT Plus EdU Alexa Fluor 647 Flow Cytometry Assay Kit; Thermo Fisher). All samples were analyzed and sorted using an Aria Fusion (Becton Dickinson) with 85 μ m nozzle except for scRNA-seq samples, which were collected using a FACS Aria III (Becton Dickinson) with 100 μ m nozzle. Flow cytometry data were analyzed using FlowJo v10.8 (Becton Dickinson).

Single-cell RNA-seq Library Preparation and Sequencing

Lung tissues were harvested from $Tgfb2^{F/F}$ and $Tgfb2^{F/F};Nlx2.1-cre$ mice at P7 and P14 after hyperoxia or normoxia treatment. Two pups were harvested for each genotype, exposure, and timepoint for total of 8 mice on P7 and 8 mice on P14. Single cell suspension was obtained as described above. To enrich for epithelial and mesenchymal populations for sequencing input, 1×10^5 CD45+ cells, 1×10^5 CD31+ cells, and 1×10^6 CD45-/CD31- cells were sorted for each sample and collected in 10% FBS/PBS. Sorted cells were then counted and labeled with oligonucleotide tags for multiplexing using 10x Genomics 3' CellPlex Kit Set A. All 8 biologic samples for the P7 timepoint were pooled and 60,000 cells / lane were loaded onto 2 lanes of a Chromium Next GEM Chip (10x Genomics). The same workflow was used for P14 samples with all 8 biologic samples for P14 pooled together and loaded onto 2 lanes as well. Lanes 1 and 2 were therefore technical replicates for each biologic sample and similarly lanes 3 and 4 were also technical replicates. Chromium Single Cell 3' v3.1 (10x Genomics) reagents were used for library preparation according to the manufacturer's protocol. The libraries were sequenced on an Illumina NovaSeq 6000 S4 flow cell.

Sequencing Data Processing

Fastq files were uploaded to the 10x Genomics Cloud (<https://www.10xgenomics.com/products/cloud-analysis>) and reads were aligned to the mouse reference genome mm10. The data were demultiplexed, and cells with multiple oligonucleotide tags were identified as multiplets and removed by the 10x Genomics cloud analysis function with default parameters. Raw count matrices were imported to the R

package Seurat v4.1.1⁸¹, and cells with fewer than 200 detected genes, more than 7500 detected genes, or more than 15% mitochondria genes were excluded. We used the DoubletFinder package⁸² for each sample using an estimated multiple rate of 1% remove doublets that were not detected upon alignment. We then merged all the sample objects, identified the top variable genes using Seurat's *FindVariableGenes* function, and integrated the samples using the *RunFastMNN* function of the SeuratWrappers R package⁸³. For visualization, Seurat's *RunUMAP* function was performed using MNN dimensional reduction.

Twenty-three clusters were initially identified from a total of 27,839 cells using Seurat's *FindNeighbors* and *FindClusters* functions with resolution = 0.3. The expression of canonical lineage markers (Epcam, Col1a1, Pecam1, Ptprc, Msln) was used to define major cell types of the lung (epithelium, mesenchyme, hematopoietic, endothelium, mesothelium). Cluster 9 (729 cells) was identified as a contaminant and excluded from further analysis due to cells showing up in multiple locations across the UMAP embedding. While re-clustering and annotating epithelial, hematopoietic, and endothelial subpopulations we identified an additional 500 cells that clustered independently from known cell types within each subcluster, had less than 1000 detected genes, and were enriched for the expression of multiple canonical cell types, suggesting these cells were also contaminants. After removing these cells and cluster 9 cells, the remaining 26,610 cells were re-clustered with *FindVariableGenes*, *RunFastMNN*, *RunUMAP*, *FindNeighbors*, and *FindClusters* functions with clustering resolution = 0.8. Thirty clusters were identified at this stage and differentially expressed genes for each cluster were identified using *FindAllMarkers* focusing on genes expressed by more than 20% of cells (either within or outside of a cluster) and with a log fold change greater than 0.2. Using publicly available data, we were able to merge and annotate clusters to obtain the 25 clusters depicted in this study. Mesenchymal cells were re-clustered using the same workflow outlined above with clustering resolution = 0.3. Clusters were annotated based on a combination of three publicly available data sets for the neonatal lung.

For Qiagen Ingenuity Pathway Analysis (Qiagen, <https://digitalinsights.qiagen.com/IPA>)⁵¹, differentially expressed genes in myofibroblasts were identified by comparing either CTRL RA vs O2 cells or RA CTRL vs cKO cells using Seurat's *FindMarkers* function. These lists were uploaded to Qiagen IPA to identify predicted upstream regulators for each comparison. To identify shared predicted upstream regulators, lists were filtered for z-score >1.5 (upregulated) or z-score <-1.5 (downregulated), and the filtered results were compared by Venn diagram between the two comparisons.

NicheNet⁵³ was used to compare signaling between conditions, as described in the “Differential NicheNet analysis between conditions of interest” vignette on the GitHub repository. Standard NicheNet statistical thresholds described in the vignette were used in the analysis. Alveolar epithelial subtypes (AT2, AT2 Lyz1, AT2 Activated, AT1/AT2, and Prolif. AT2) were used as a combined sender cell population, and alveolar and ductal myofibroblasts were used as combined receiver cell populations. Differential signaling from sender-to-receiver cells was compared across two conditions, CTRL RA vs CTRL O2 and CTRL RA vs cKO RA, and the results were examined for pathways present in both comparisons.

Data Analysis

Mean linear intercept morphometry was quantified using ImageJ software as described previously⁸⁰. scRNA-seq data analysis was performed in R version 4.1.1. Statistical tests were performed in GraphPad Prism version 9.4.0.

Data Availability

The data that support this study are available upon reasonable request. Sequencing data and Seurat objects were deposited in the Gene Expression Omnibus Series GSE243129.

Grants

I.S.K was supported by the Pediatric Scientist Development Program, the Nina Ireland Program for Lung Health, and the UCSF Division of Neonatology. This work was supported by HD000850 (NICDH, I.S.K.); UCSF Division of Neonatology (I.S.K.); and HL145037 and HL142568 (NHLBI, D.S.).

Acknowledgements

We thank members of the Sheppard lab for helpful advice and discussion. We thank the following UCSF core facilities for their technical support: Laboratory for Cell Analysis (supported by P30CA082103), Center for Advanced Light Microscopy (supported by UCSF PBBR), Gladstone Genomics Core, Gladstone Histology and Light Microscopy Core, Gladstone Transgenic Gene Targeting Core, and the Center for Advanced Technology (supported by UCSF PBBR, RRP IMIA, and 1S10OD028511-01).

Disclosures

D.S. is a founder of Pliant Therapeutics, a member of the Genentech Scientific Review Board, a member of the Amgen Immunology Scientific Advisory Board, and a member of the Scientific Review Board for Lila Biologics. No funding or reagents from any of these companies were used for this project. None of the other authors has any conflicts of interest, financial or otherwise, to disclose.

Author Contributions

I.S.K and D.S. conceived the study, interpreted the data, and wrote the manuscript. I.S.K., C.M., X.R., V.A., and M.C. performed the experiments and/or analyzed the data. T.T. and A.A. provided critical resources for this study. D.S. supervised the study.

References

1. Jobe AJ. The new BPD: an arrest of lung development. *Pediatr Res* 1999;46:641-3.
2. Thebaud B, Goss KN, Laughon M, et al. Bronchopulmonary dysplasia. *Nat Rev Dis Primers* 2019;5:78.
3. Northway WH, Jr., Rosan RC, Porter DY. Pulmonary disease following respirator therapy of hyaline-membrane disease. Bronchopulmonary dysplasia. *N Engl J Med* 1967;276:357-68.
4. Oak P, Hilgendorff A. The BPD trio? Interaction of dysregulated PDGF, VEGF, and TGF signaling in neonatal chronic lung disease. *Mol Cell Pediatr* 2017;4:11.
5. Saito A, Horie M, Nagase T. TGF-beta Signaling in Lung Health and Disease. *Int J Mol Sci* 2018;19.
6. Surate Solaligue DE, Rodriguez-Castillo JA, Ahlbrecht K, Morty RE. Recent advances in our understanding of the mechanisms of late lung development and bronchopulmonary dysplasia. *Am J Physiol Lung Cell Mol Physiol* 2017;313:L1101-L53.
7. Mizikova I, Morty RE. The Extracellular Matrix in Bronchopulmonary Dysplasia: Target and Source. *Front Med (Lausanne)* 2015;2:91.
8. Alejandre-Alcazar MA, Kwapiszewska G, Reiss I, et al. Hyperoxia modulates TGF-beta/BMP signaling in a mouse model of bronchopulmonary dysplasia. *Am J Physiol Lung Cell Mol Physiol* 2007;292:L537-49.
9. Nakanishi H, Sugiura T, Streisand JB, Lonning SM, Roberts JD, Jr. TGF-beta-neutralizing antibodies improve pulmonary alveogenesis and vasculogenesis in the injured newborn lung. *Am J Physiol Lung Cell Mol Physiol* 2007;293:L151-61.
10. Vento G, Capoluongo E, Matassa PG, et al. Serum levels of seven cytokines in premature ventilated newborns: correlations with old and new forms of bronchopulmonary dysplasia. *Intensive Care Med* 2006;32:723-30.
11. Jonsson B, Li YH, Noack G, Brauner A, Tullus K. Downregulatory cytokines in tracheobronchial aspirate fluid from infants with chronic lung disease of prematurity. *Acta Paediatr* 2000;89:1375-80.
12. Kotecha S, Wangoo A, Silverman M, Shaw RJ. Increase in the concentration of transforming growth factor beta-1 in bronchoalveolar lavage fluid before development of chronic lung disease of prematurity. *J Pediatr* 1996;128:464-9.
13. Lecart C, Cayabyab R, Buckley S, et al. Bioactive transforming growth factor-beta in the lungs of extremely low birthweight neonates predicts the need for home oxygen supplementation. *Biol Neonate* 2000;77:217-23.
14. Mizikova I, Ruiz-Camp J, Steenbock H, et al. Collagen and elastin cross-linking is altered during aberrant late lung development associated with hyperoxia. *Am J Physiol Lung Cell Mol Physiol* 2015;308:L1145-58.
15. Witsch TJ, Niess G, Sakkas E, et al. Transglutaminase 2: a new player in bronchopulmonary dysplasia? *Eur Respir J* 2014;44:109-21.
16. Witsch TJ, Turowski P, Sakkas E, et al. Deregulation of the lysyl hydroxylase matrix cross-linking system in experimental and clinical bronchopulmonary dysplasia. *Am J Physiol Lung Cell Mol Physiol* 2014;306:L246-59.

17. Rath P, Nardiello C, Surate Solaligue DE, et al. Caffeine administration modulates TGF-beta signaling but does not attenuate blunted alveolarization in a hyperoxia-based mouse model of bronchopulmonary dysplasia. *Pediatr Res* 2017;81:795-805.
18. Ahlfeld SK, Wang J, Gao Y, Snider P, Conway SJ. Initial Suppression of Transforming Growth Factor-beta Signaling and Loss of TGFB1 Causes Early Alveolar Structural Defects Resulting in Bronchopulmonary Dysplasia. *Am J Pathol* 2016;186:777-93.
19. Chen H, Sun J, Buckley S, et al. Abnormal mouse lung alveolarization caused by Smad3 deficiency is a developmental antecedent of centrilobular emphysema. *Am J Physiol Lung Cell Mol Physiol* 2005;288:L683-91.
20. Kulkarni AB, Huh CG, Becker D, et al. Transforming growth factor beta 1 null mutation in mice causes excessive inflammatory response and early death. *Proc Natl Acad Sci U S A* 1993;90:770-4.
21. Li A, Ma S, Smith SM, et al. Mesodermal ALK5 controls lung myofibroblast versus lipofibroblast cell fate. *BMC Biol* 2016;14:19.
22. Li M, Li C, Liu YH, et al. Mesodermal deletion of transforming growth factor-beta receptor II disrupts lung epithelial morphogenesis: cross-talk between TGF-beta and Sonic hedgehog pathways. *J Biol Chem* 2008;283:36257-64.
23. Miao Q, Chen H, Luo Y, et al. Abrogation of mesenchyme-specific TGF-beta signaling results in lung malformation with prenatal pulmonary cysts in mice. *Am J Physiol Lung Cell Mol Physiol* 2021;320:L1158-L68.
24. Noe N, Shim A, Millette K, et al. Mesenchyme-specific deletion of Tgf-beta1 in the embryonic lung disrupts branching morphogenesis and induces lung hypoplasia. *Lab Invest* 2019;99:1363-75.
25. Plosa EJ, Young LR, Gulleman PM, et al. Epithelial beta1 integrin is required for lung branching morphogenesis and alveolarization. *Development* 2014;141:4751-62.
26. Sureshbabu A, Syed MA, Boddupalli CS, et al. Conditional overexpression of TGFbeta1 promotes pulmonary inflammation, apoptosis and mortality via TGFbetaR2 in the developing mouse lung. *Respir Res* 2015;16:4.
27. Colarossi C, Chen Y, Obata H, et al. Lung alveolar septation defects in Ltbp-3-null mice. *Am J Pathol* 2005;167:419-28.
28. Chen H, Zhuang F, Liu YH, et al. TGF-beta receptor II in epithelia versus mesenchyme plays distinct roles in the developing lung. *Eur Respir J* 2008;32:285-95.
29. Gao F, Li C, Danopoulos S, et al. Hedgehog-responsive PDGFRa(+) fibroblasts maintain a unique pool of alveolar epithelial progenitor cells during alveogenesis. *Cell Rep* 2022;39:110608.
30. Frangogiannis N. Transforming growth factor-beta in tissue fibrosis. *J Exp Med* 2020;217:e20190103.
31. Li R, Bernau K, Sandbo N, Gu J, Preissl S, Sun X. Pdgfra marks a cellular lineage with distinct contributions to myofibroblasts in lung maturation and injury response. *Elife* 2018;7.
32. Li C, Li M, Li S, et al. Progenitors of secondary crest myofibroblasts are developmentally committed in early lung mesoderm. *Stem Cells* 2015;33:999-1012.
33. Ushakumary MG, Riccetti M, Perl AT. Resident interstitial lung fibroblasts and their role in alveolar stem cell niche development, homeostasis, injury, and regeneration. *Stem Cells Transl Med* 2021;10:1021-32.

34. Branchfield K, Li R, Lungova V, Verheyden JM, McCulley D, Sun X. A three-dimensional study of alveologenesis in mouse lung. *Dev Biol* 2016;409:429-41.
35. Hagan AS, Zhang B, Ornitz DM. Identification of a FGF18-expressing alveolar myofibroblast that is developmentally cleared during alveologenesis. *Development* 2020;147.
36. Riccetti MR, Ushakumary MG, Waltamath M, et al. Maladaptive functional changes in alveolar fibroblasts due to perinatal hyperoxia impair epithelial differentiation. *JCI Insight* 2022;7.
37. Li R, Li X, Hagood J, Zhu MS, Sun X. Myofibroblast contraction is essential for generating and regenerating the gas-exchange surface. *J Clin Invest* 2020;130:2859-71.
38. Benjamin JT, Smith RJ, Halloran BA, Day TJ, Kelly DR, Prince LS. FGF-10 is decreased in bronchopulmonary dysplasia and suppressed by Toll-like receptor activation. *Am J Physiol Lung Cell Mol Physiol* 2007;292:L550-8.
39. Bozyk PD, Bentley JK, Popova AP, et al. Neonatal periostin knockout mice are protected from hyperoxia-induced alveolar simplification. *PLoS One* 2012;7:e31336.
40. Popova AP, Bentley JK, Cui TX, et al. Reduced platelet-derived growth factor receptor expression is a primary feature of human bronchopulmonary dysplasia. *Am J Physiol Lung Cell Mol Physiol* 2014;307:L231-9.
41. Mund SI, Stampanoni M, Schittny JC. Developmental alveolarization of the mouse lung. *Dev Dyn* 2008;237:2108-16.
42. Schittny JC. Development of the lung. *Cell Tissue Res* 2017;367:427-44.
43. Vila Ellis L, Chen J. A cell-centric view of lung alveologenesis. *Dev Dyn* 2021;250:482-96.
44. Liu L, Mao Q, Chu S, et al. Intranasal versus intraperitoneal delivery of human umbilical cord tissue-derived cultured mesenchymal stromal cells in a murine model of neonatal lung injury. *Am J Pathol* 2014;184:3344-58.
45. Tsujino K, Li JT, Tsukui T, et al. Fra-2 negatively regulates postnatal alveolar septation by modulating myofibroblast function. *Am J Physiol Lung Cell Mol Physiol* 2017;313:L878-L88.
46. Yee M, Chess PR, McGrath-Morrow SA, et al. Neonatal oxygen adversely affects lung function in adult mice without altering surfactant composition or activity. *Am J Physiol Lung Cell Mol Physiol* 2009;297:L641-9.
47. Hurskainen M, Mizikova I, Cook DP, et al. Single cell transcriptomic analysis of murine lung development on hyperoxia-induced damage. *Nat Commun* 2021;12:1565.
48. Negretti NM, Plosa EJ, Benjamin JT, et al. A single-cell atlas of mouse lung development. *Development* 2021;148.
49. Narvaez Del Pilar O, Gacha Garay MJ, Chen J. Three-axis classification of mouse lung mesenchymal cells reveals two populations of myofibroblasts. *Development* 2022;149.
50. Xia S, Vila Ellis L, Winkley K, et al. Neonatal hyperoxia induces activated pulmonary cellular states and sex-dependent transcriptomic changes in a model of experimental bronchopulmonary dysplasia. *Am J Physiol Lung Cell Mol Physiol* 2023;324:L123-L40.
51. Kramer A, Green J, Pollard J, Jr., Tugendreich S. Causal analysis approaches in Ingenuity Pathway Analysis. *Bioinformatics* 2014;30:523-30.
52. Calthorpe RJ, Poulter C, Smyth AR, et al. Complex roles of TGF-beta signaling pathways in lung development and bronchopulmonary dysplasia. *Am J Physiol Lung Cell Mol Physiol* 2023;324:L285-L96.

53. Browaeys R, Saelens W, Saeys Y. NicheNet: modeling intercellular communication by linking ligands to target genes. *Nat Methods* 2020;17:159-62.
54. Li C, Lee MK, Gao F, et al. Secondary crest myofibroblast PDGFRalpha controls the elastogenesis pathway via a secondary tier of signaling networks during alveogenesis. *Development* 2019;146.
55. Chung MI, Bujnis M, Barkauskas CE, Kobayashi Y, Hogan BLM. Niche-mediated BMP/SMAD signaling regulates lung alveolar stem cell proliferation and differentiation. *Development* 2018;145.
56. Ahn S, Joyner AL. Dynamic changes in the response of cells to positive hedgehog signaling during mouse limb patterning. *Cell* 2004;118:505-16.
57. Morris DG, Huang X, Kaminski N, et al. Loss of integrin alpha(v)beta6-mediated TGF-beta activation causes Mmp12-dependent emphysema. *Nature* 2003;422:169-73.
58. Munger JS, Huang X, Kawakatsu H, et al. The integrin alpha v beta 6 binds and activates latent TGF beta 1: a mechanism for regulating pulmonary inflammation and fibrosis. *Cell* 1999;96:319-28.
59. Yokosaki Y, Monis H, Chen J, Sheppard D. Differential effects of the integrins alpha9beta1, alphavbeta3, and alphavbeta6 on cell proliferative responses to tenascin. Roles of the beta subunit extracellular and cytoplasmic domains. *J Biol Chem* 1996;271:24144-50.
60. Huang XZ, Wu JF, Cass D, et al. Inactivation of the integrin beta 6 subunit gene reveals a role of epithelial integrins in regulating inflammation in the lung and skin. *J Cell Biol* 1996;133:921-8.
61. Hogmalm A, Sheppard D, Lappalainen U, Bry K. beta6 Integrin subunit deficiency alleviates lung injury in a mouse model of bronchopulmonary dysplasia. *Am J Respir Cell Mol Biol* 2010;43:88-98.
62. Massague J, Sheppard D. TGF-beta signaling in health and disease. *Cell* 2023;186:4007-37.
63. Henderson NC, Arnold TD, Katamura Y, et al. Targeting of alphav integrin identifies a core molecular pathway that regulates fibrosis in several organs. *Nat Med* 2013;19:1617-24.
64. Reed NI, Jo H, Chen C, et al. The alphavbeta1 integrin plays a critical in vivo role in tissue fibrosis. *Sci Transl Med* 2015;7:288ra79.
65. Mu D, Cambier S, Fjellbirkeland L, et al. The integrin alpha(v)beta8 mediates epithelial homeostasis through MT1-MMP-dependent activation of TGF-beta1. *J Cell Biol* 2002;157:493-507.
66. Cook DR, Solski PA, Bultman SJ, et al. The ect2 rho Guanine nucleotide exchange factor is essential for early mouse development and normal cell cytokinesis and migration. *Genes Cancer* 2011;2:932-42.
67. Kimani PW, Holmes AJ, Grossmann RE, McGowan SE. PDGF-Ralpha gene expression predicts proliferation, but PDGF-A suppresses transdifferentiation of neonatal mouse lung myofibroblasts. *Respir Res* 2009;10:119.
68. Zhang K, Yao E, Chen B, et al. Acquisition of cellular properties during alveolar formation requires differential activity and distribution of mitochondria. *Elife* 2022;11.
69. McGowan SE, McCoy DM. Regulation of fibroblast lipid storage and myofibroblast phenotypes during alveolar septation in mice. *Am J Physiol Lung Cell Mol Physiol* 2014;307:L618-31.
70. Oak P, Pritzke T, Thiel I, et al. Attenuated PDGF signaling drives alveolar and microvascular defects in neonatal chronic lung disease. *EMBO Mol Med* 2017;9:1504-20.

71. Kugler MC, Loomis CA, Zhao Z, Cushman JC, Liu L, Munger JS. Sonic Hedgehog Signaling Regulates Myofibroblast Function during Alveolar Septum Formation in Murine Postnatal Lung. *Am J Respir Cell Mol Biol* 2017;57:280-93.
72. Yie TA, Loomis CA, Nowatzky J, et al. Hedgehog and Platelet-derived Growth Factor Signaling Intersect during Postnatal Lung Development. *Am J Respir Cell Mol Biol* 2023;68:523-36.
73. Pittet JF, Griffiths MJ, Geiser T, et al. TGF-beta is a critical mediator of acute lung injury. *J Clin Invest* 2001;107:1537-44.
74. Breuss JM, Gillett N, Lu L, Sheppard D, Pytela R. Restricted distribution of integrin beta 6 mRNA in primate epithelial tissues. *J Histochem Cytochem* 1993;41:1521-7.
75. Kumarasamy A, Schmitt I, Nave AH, et al. Lysyl oxidase activity is dysregulated during impaired alveolarization of mouse and human lungs. *Am J Respir Crit Care Med* 2009;180:1239-52.
76. Bry K, Whitsett JA, Lappalainen U. IL-1beta disrupts postnatal lung morphogenesis in the mouse. *Am J Respir Cell Mol Biol* 2007;36:32-42.
77. Tsukui T, Sun KH, Wetter JB, et al. Collagen-producing lung cell atlas identifies multiple subsets with distinct localization and relevance to fibrosis. *Nat Commun* 2020;11:1920.
78. Chytil A, Magnuson MA, Wright CV, Moses HL. Conditional inactivation of the TGF-beta type II receptor using Cre:Lox. *Genesis* 2002;32:73-5.
79. Dasch JR, Pace DR, Waegell W, Inenaga D, Ellingsworth L. Monoclonal antibodies recognizing transforming growth factor-beta. Bioactivity neutralization and transforming growth factor beta 2 affinity purification. *J Immunol* 1989;142:1536-41.
80. Crowley G, Kwon S, Caraher EJ, et al. Quantitative lung morphology: semi-automated measurement of mean linear intercept. *BMC Pulm Med* 2019;19:206.
81. Hao Y, Hao S, Andersen-Nissen E, et al. Integrated analysis of multimodal single-cell data. *Cell* 2021;184:3573-87 e29.
82. McGinnis CS, Murrow LM, Gartner ZJ. DoubletFinder: Doublet Detection in Single-Cell RNA Sequencing Data Using Artificial Nearest Neighbors. *Cell Syst* 2019;8:329-37 e4.
83. Butler A, Hoffman P, Smibert P, Papalexi E, Satija R. Integrating single-cell transcriptomic data across different conditions, technologies, and species. *Nat Biotechnol* 2018;36:411-20.

Figure 1

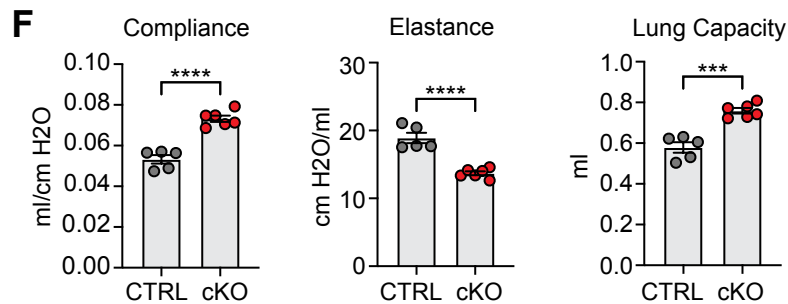
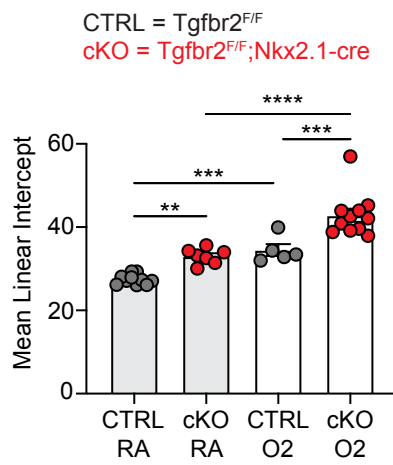
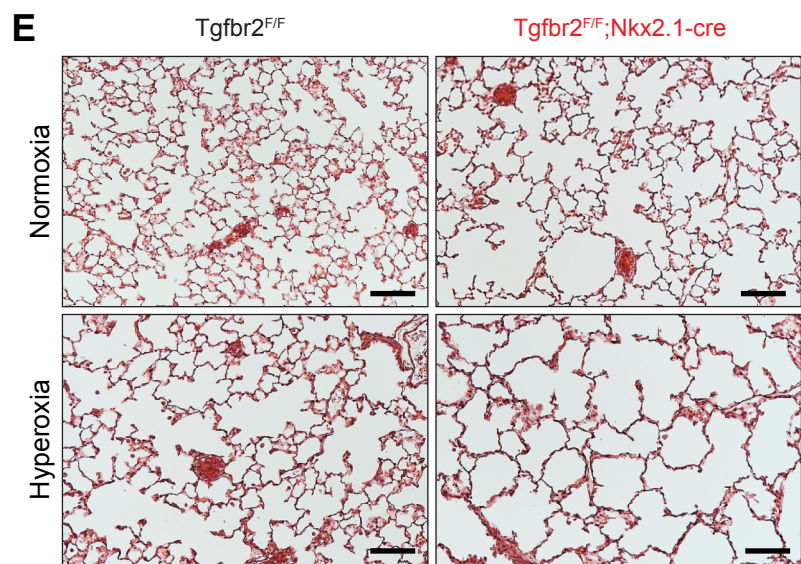
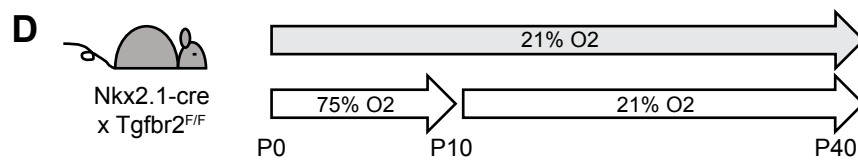
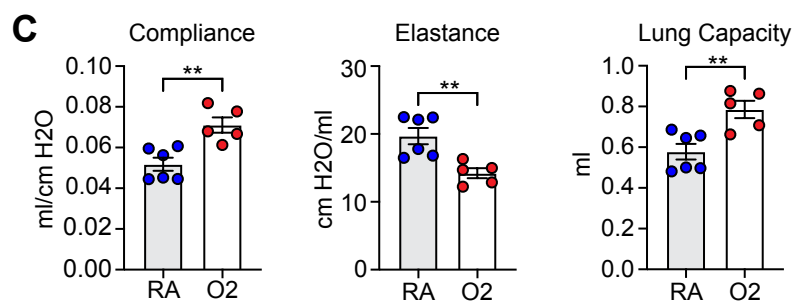
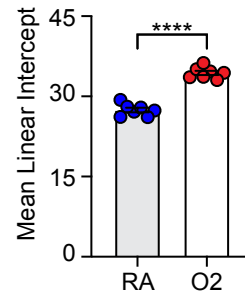
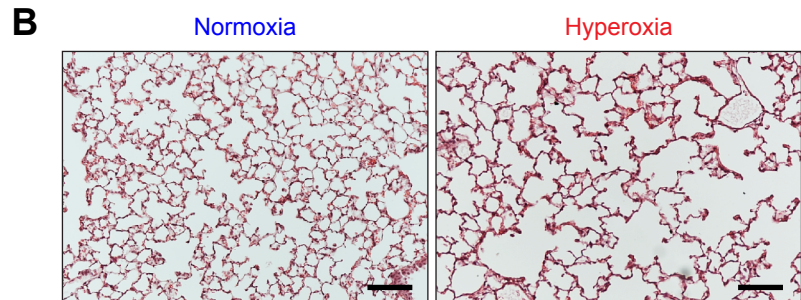
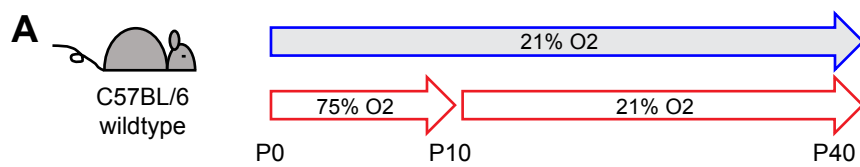
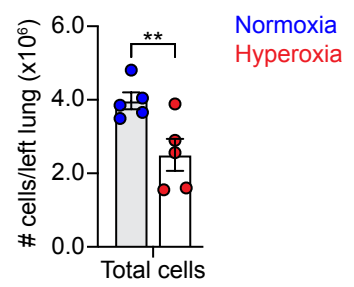
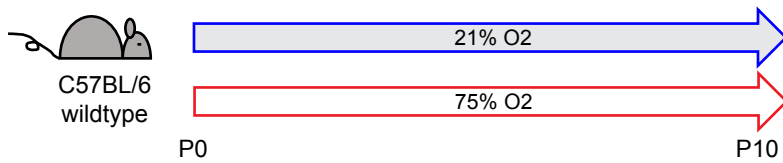


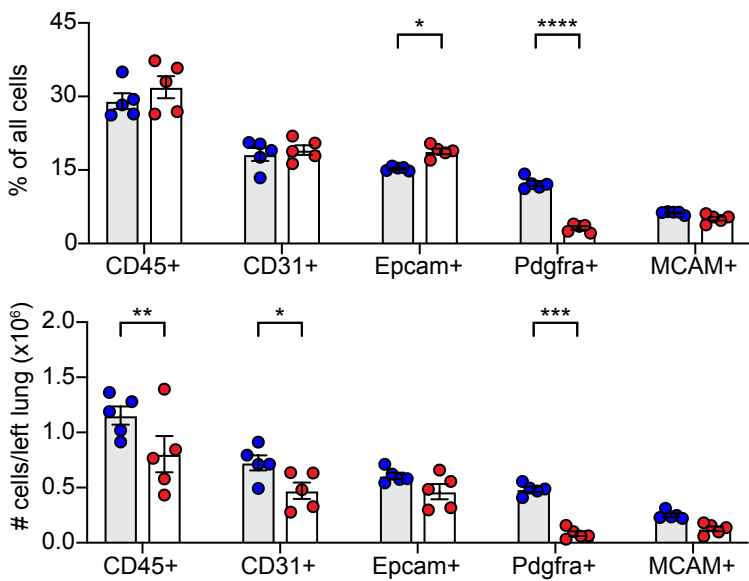
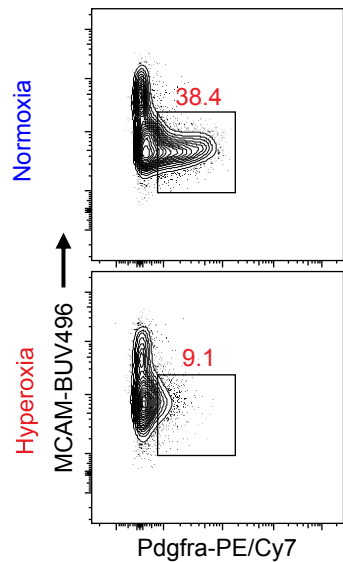
Figure 2

A

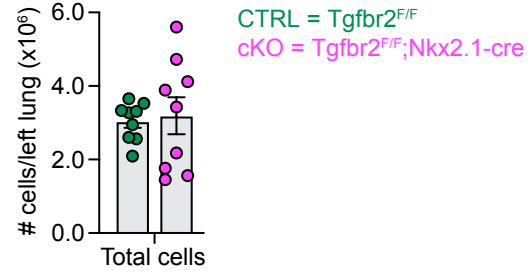
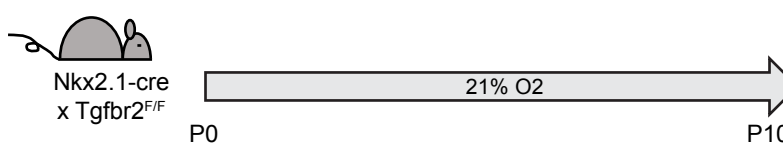


B

Gate: Live cells, CD45-, CD31-, Epcam-



C



D

Gate: Live cells, CD45-, CD31-, Epcam-

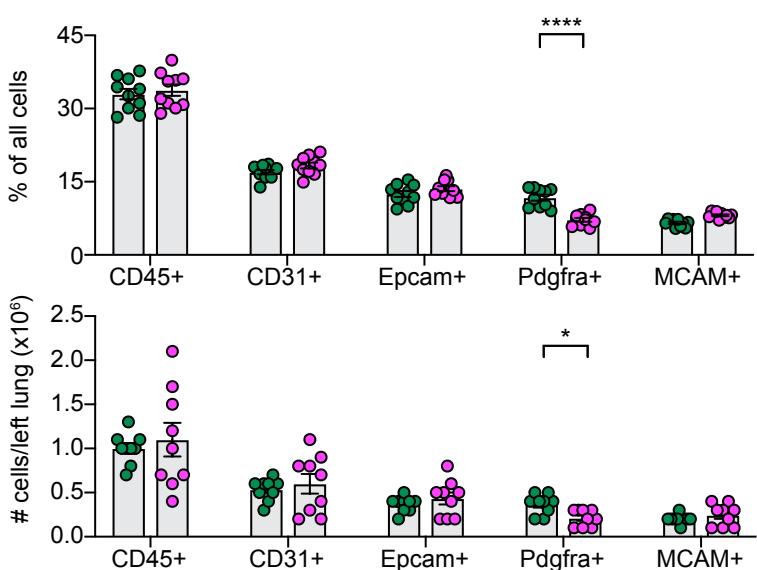
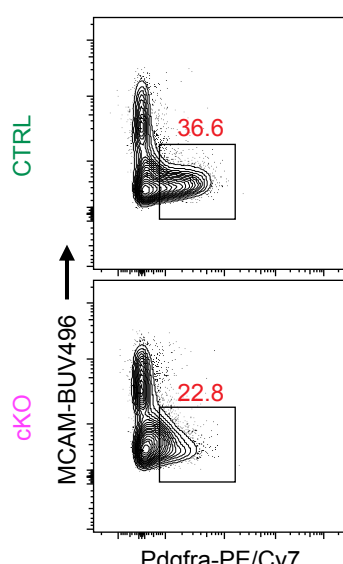


Figure 3

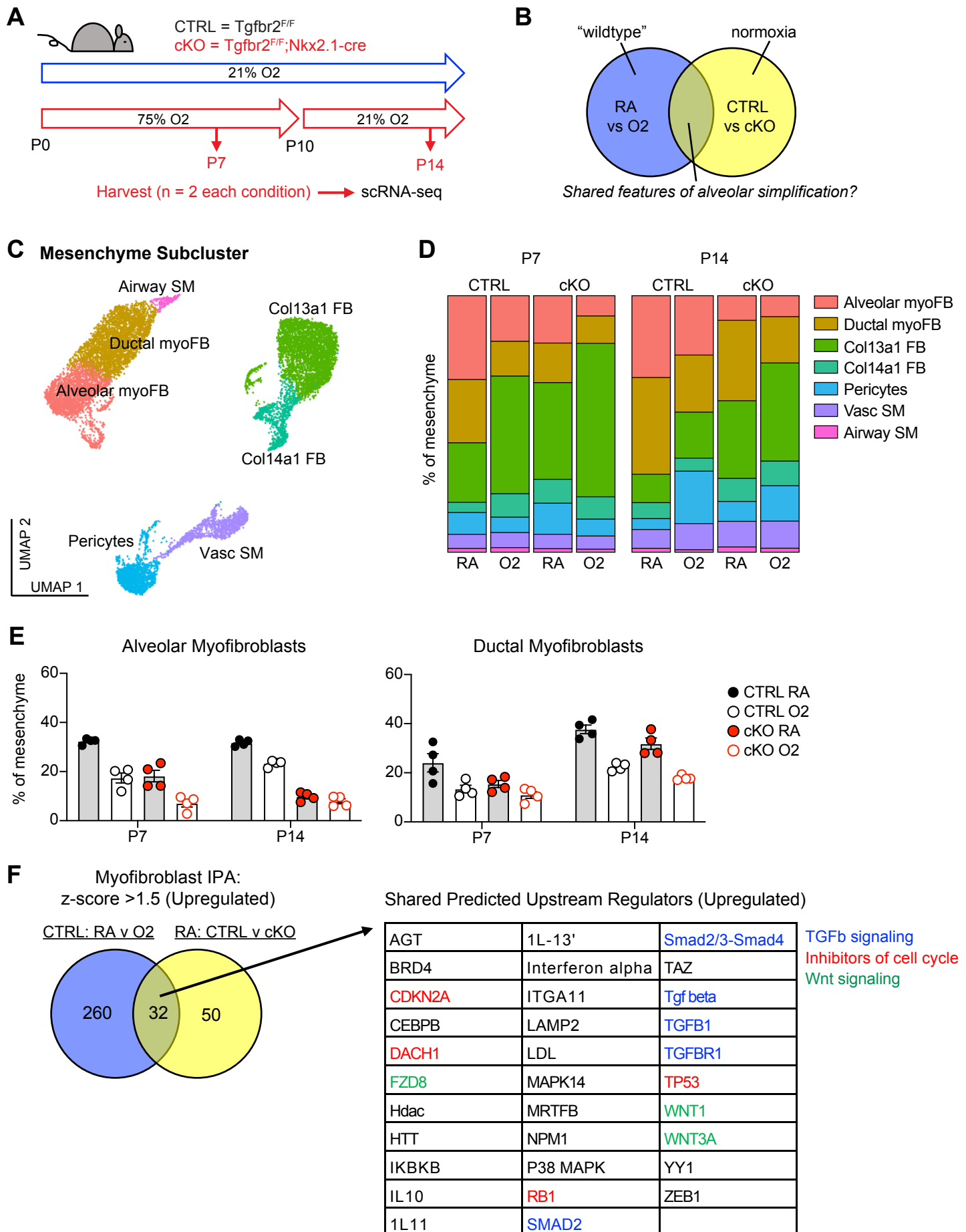
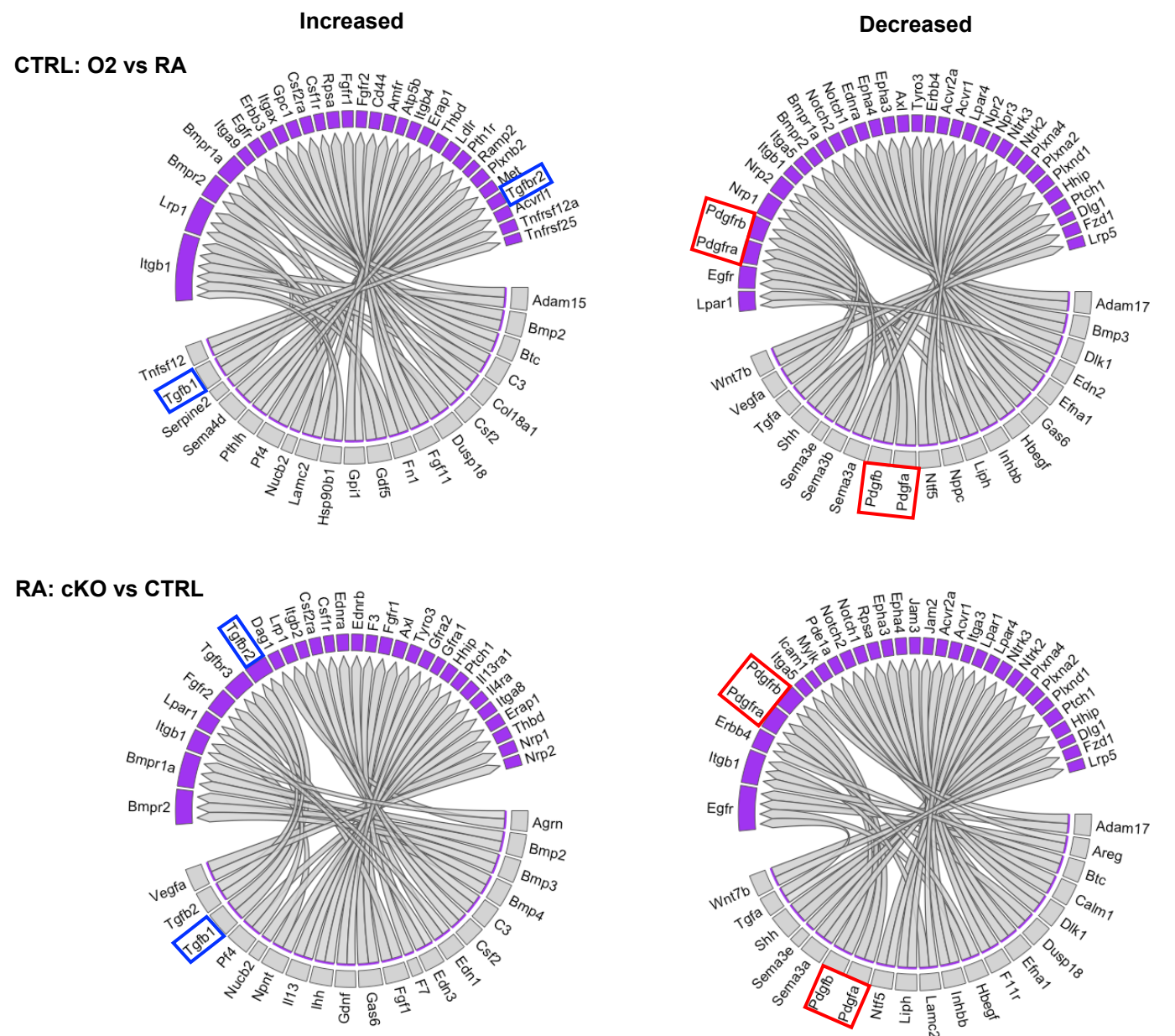


Figure 4

A Alveolar Epithelium to Myofibroblasts



B

Shared Increased:

Tgfb1-Tgfb2
 Ptf4-Thbd
 Nucb2-Erap1
 Csf2-Csf2ra
 Csf2-Csf1r
 C3-Lrp1
 Bmp2-Bmpr2
 Bmp2-Bmpr1a

Shared Decreased:

Wnt7b-Lrp5
Wnt7b-Fzd1
Tgfa-Egfr
Tgfa-Dlg1
Shh-Ptch1
Shh-Hhip
Sema3e-Plxnd1
Sema3a-Plxna2
Sema3a-Plxna4
Pdgfa-Pdgfra
Pdgfa-Pdgfrb
Pdgfb-Pdgfra
Pdgfb-Pdgfrb
Ntf5-Ntrk2
Ntf5-Ntrk3
Liph-Lpar1
Liph-Lpar4
Inhbb-Acvr1
Inhbb-Acvr2a
Hbegf-Egfr
Hbegf-Erb4
Efna1-Epha3
Efna1-Epha4
Dlk1-Notch2
Dlk1-Notch3
Adam17-Itga5
Adam17-Itgb1

Figure 5

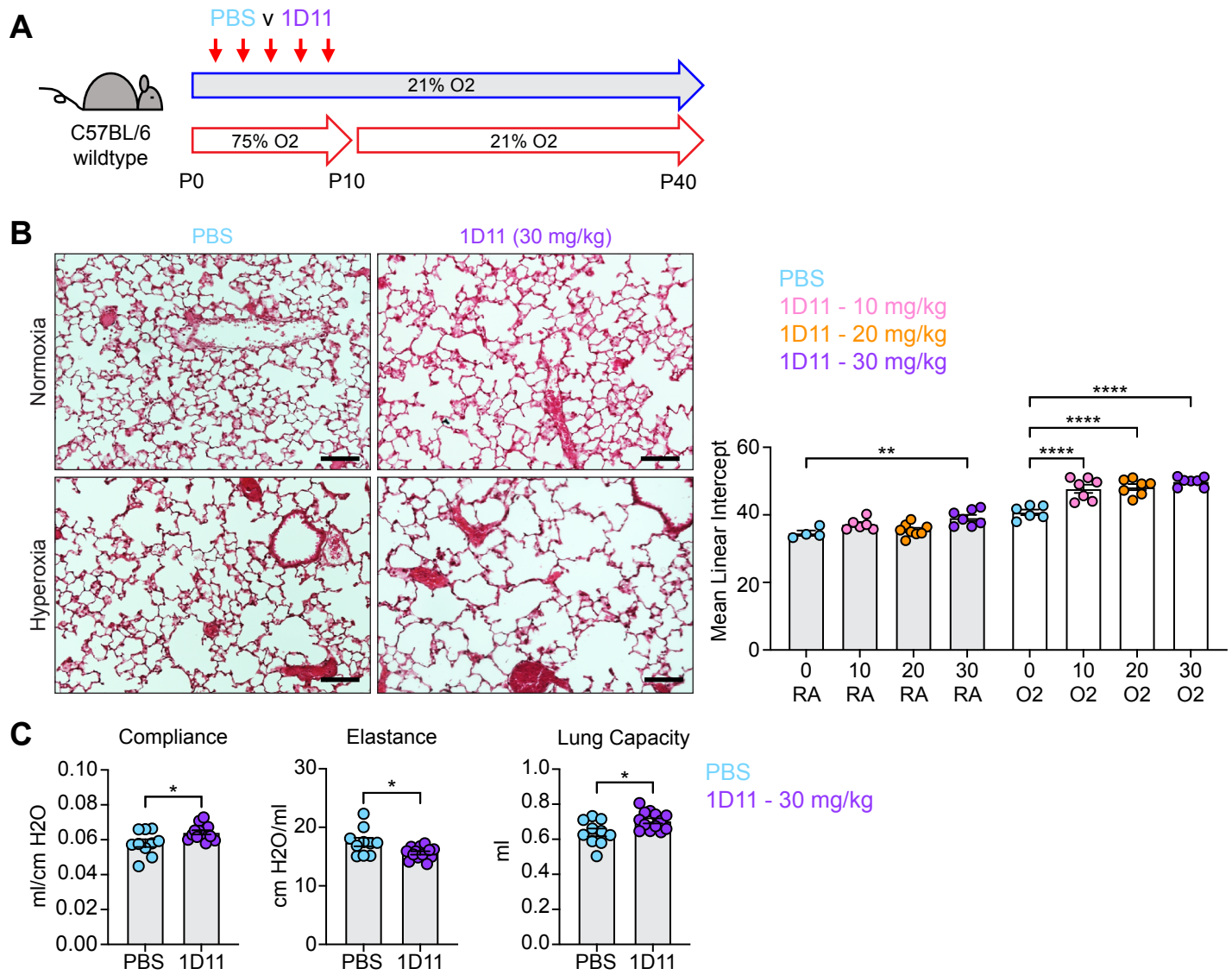


Figure 6

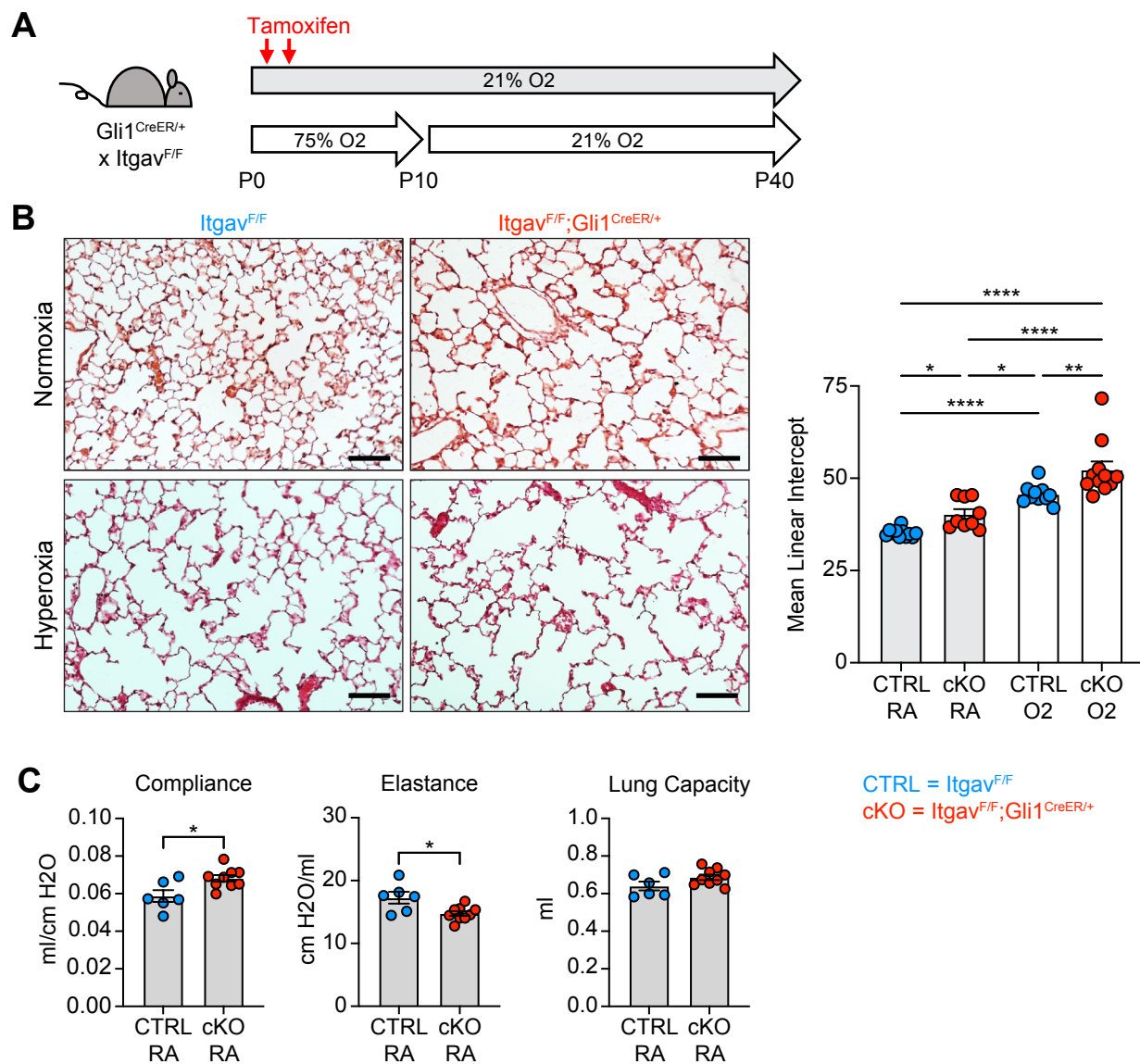


Figure 7

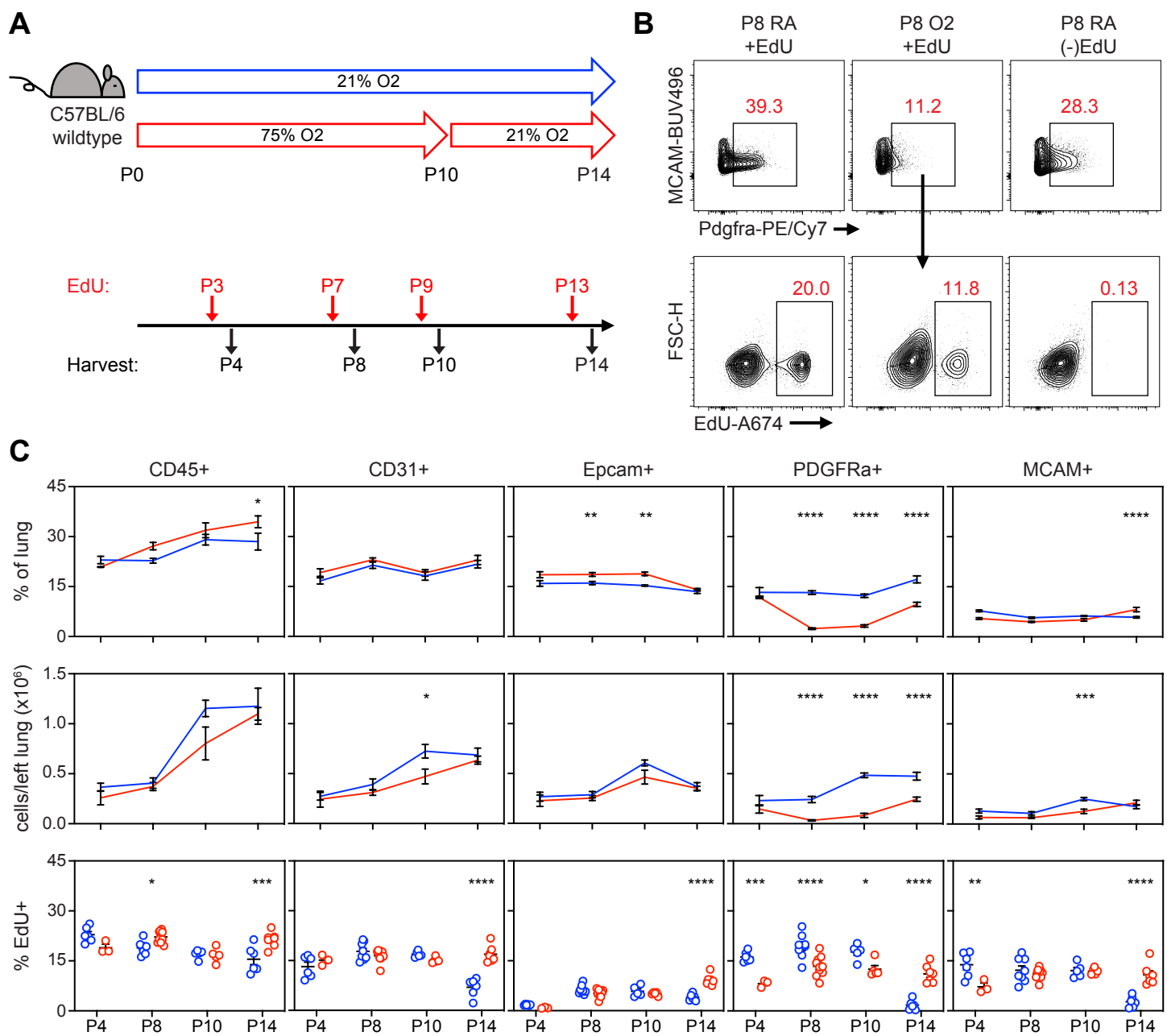
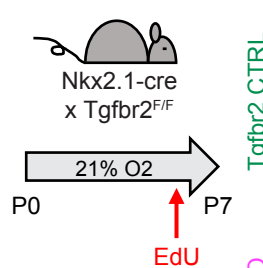
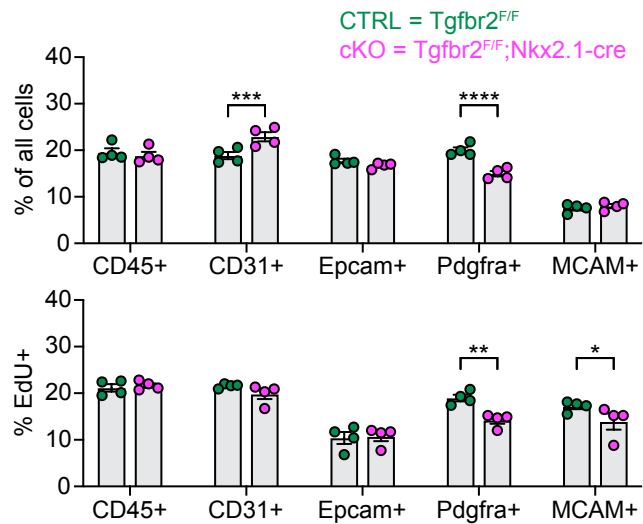
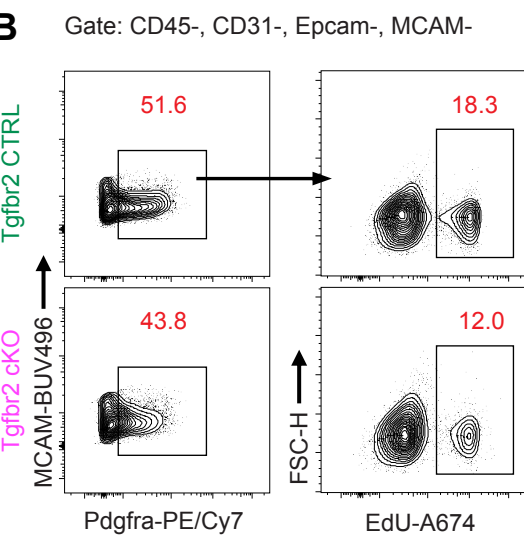


Figure 8

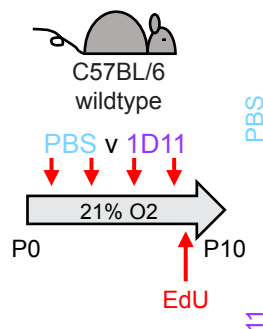
A



B



C



D

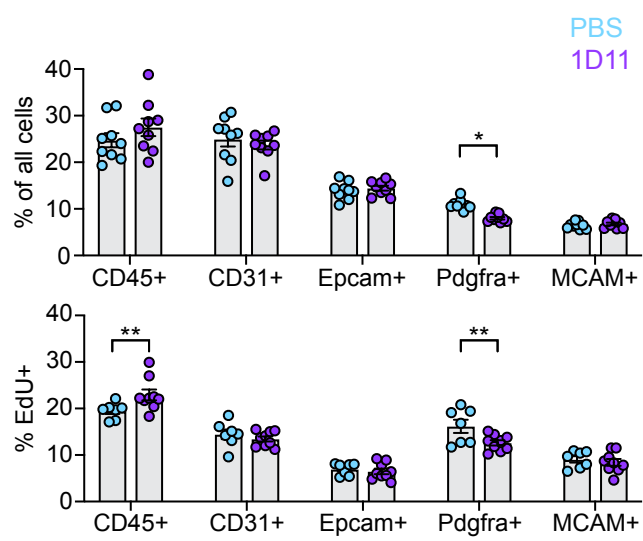
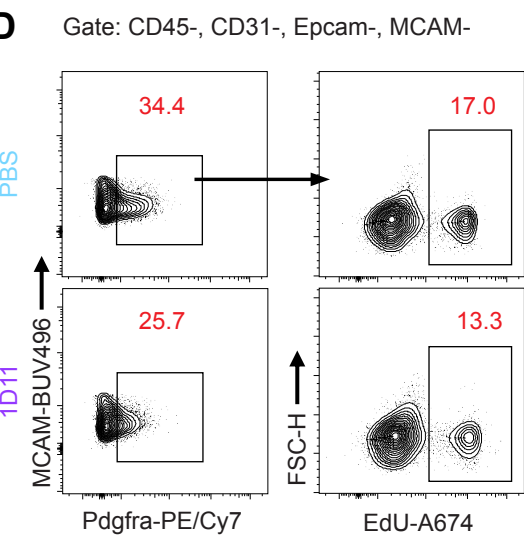
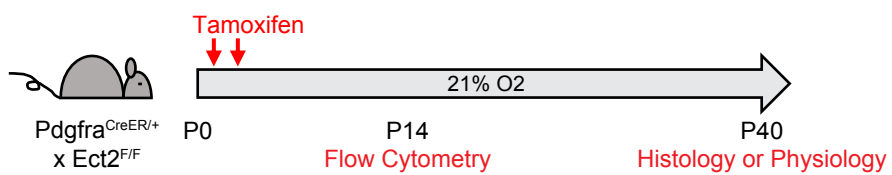
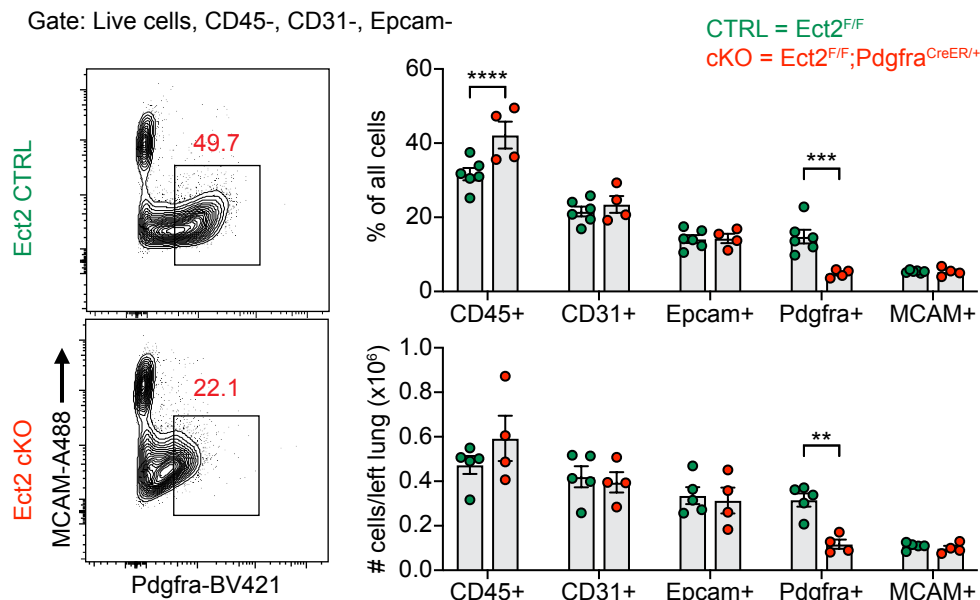


Figure 9

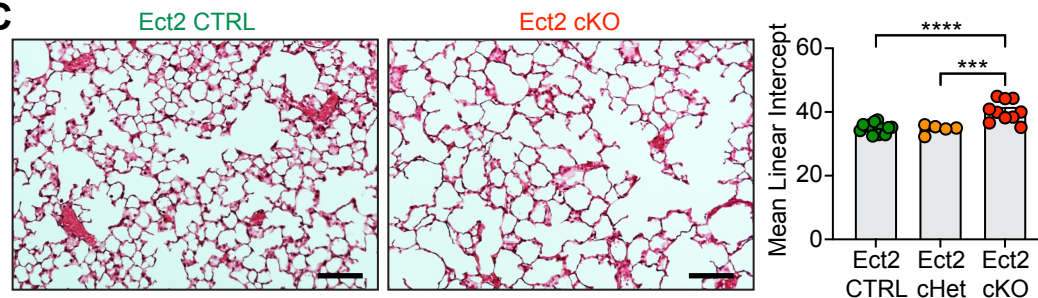
A



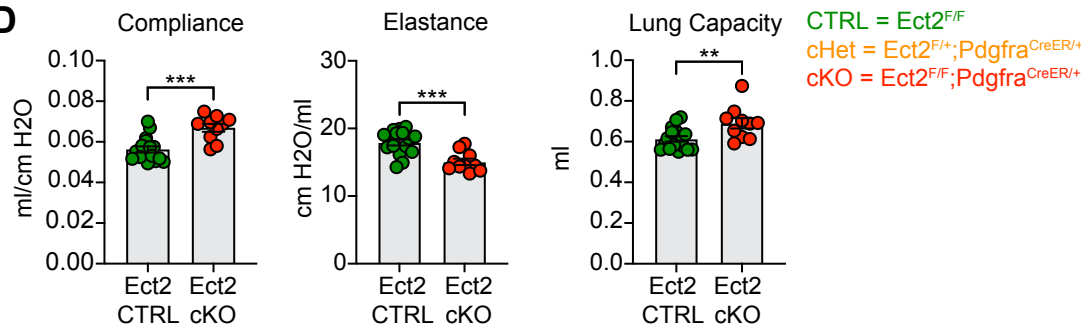
B



C

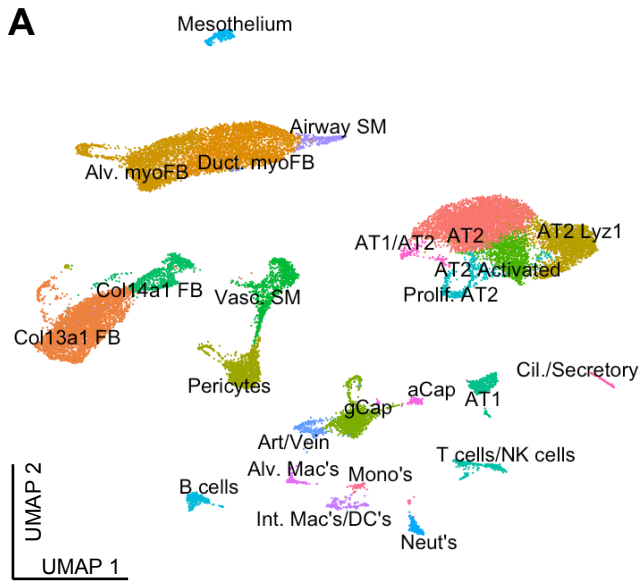


D

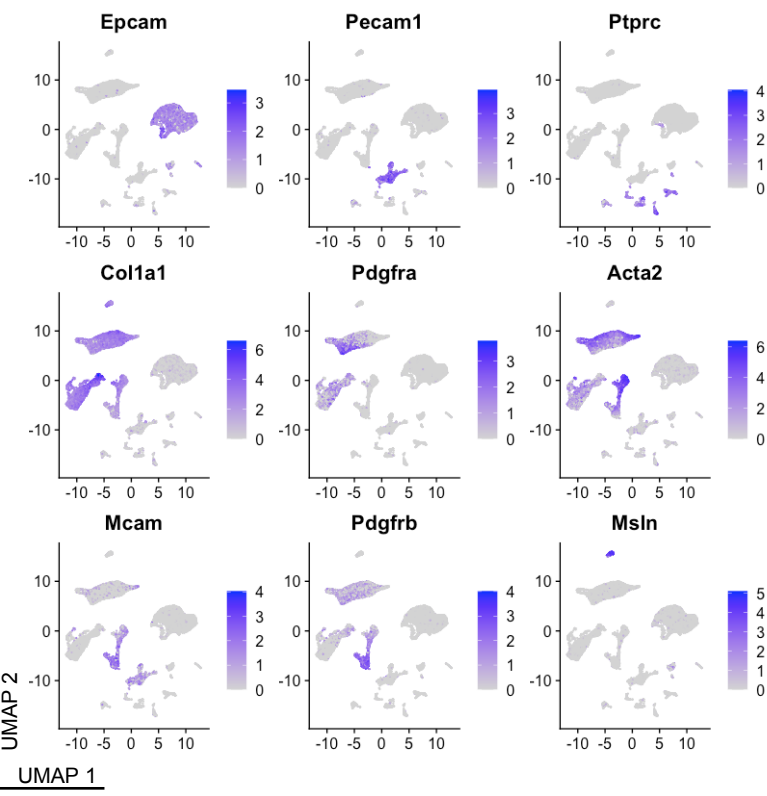


Supplementary Figure 1

A



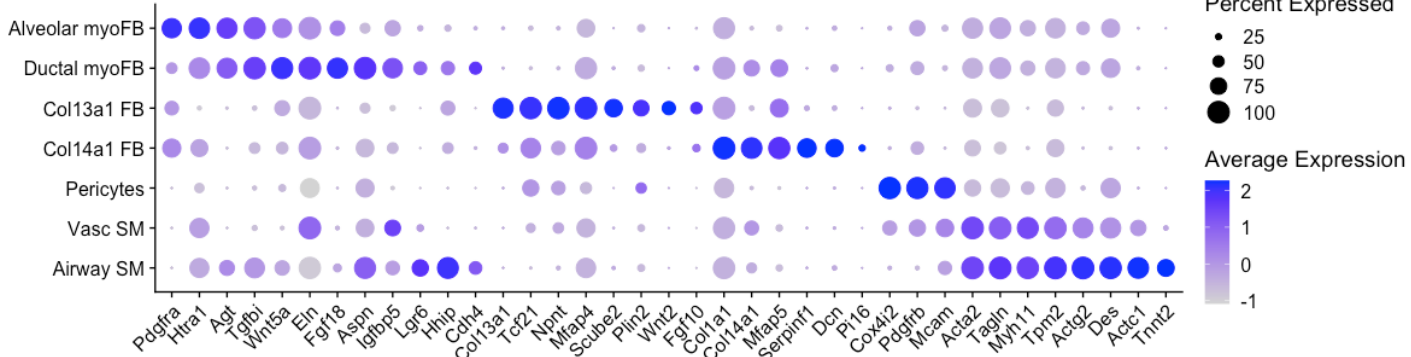
B



C

Subset	Cells
Mesenchyme	13,331
Epithelium	9,262
Endothelium	1,856
Hematopoietic	1,798
Mesothelium	363
Total	26,610

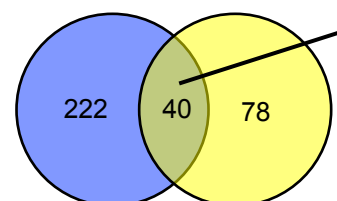
D



E

Myofibroblast IPA:
z-score <-1.5 (Downregulated)

CTRL: RA v O2 RA: CTRL v cKO

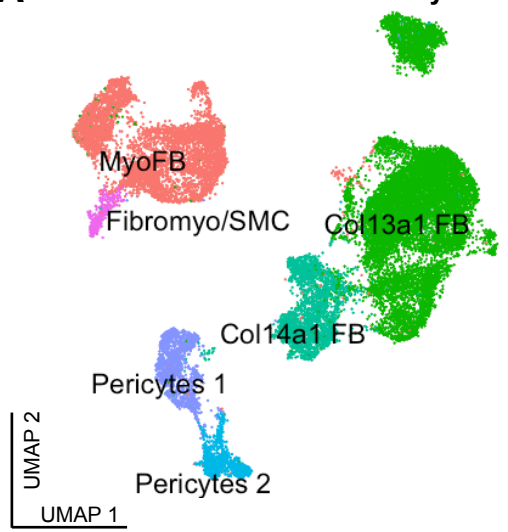


Shared Predicted Upstream Regulators (Downregulated)

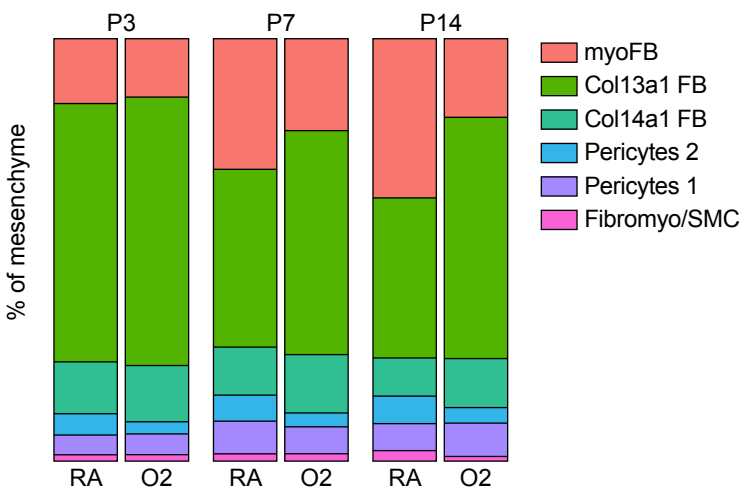
ADAM12	GNAS	MEF2C	PPARG
ALDH1A2	GPER1	miR-30c-5p	RELA
APEX1	HDAC2	NANOG	SMAD7
BDNF	HGF	NCOA2	TLR3
COL5A1	IFNG	NFKB (complex)	TNF
CREB1	IL1B	NGF	TSC2
CTNNB1	LEP	NOD2	Vegf
ELK1	LIF	NRAS	
EPHA2	MAP2K5	PDGF BB	
FSH	MAP3K8	PDGFB	
GLI3	MAPK1	POMC	

Supplementary Figure 2

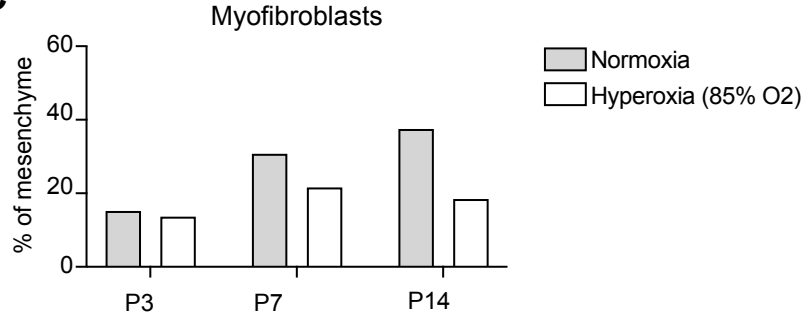
A Hurskainen et al. Mesenchyme



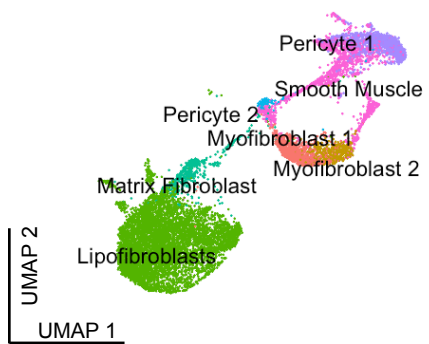
B



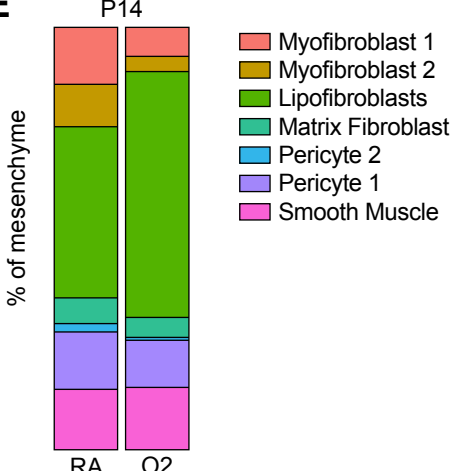
C



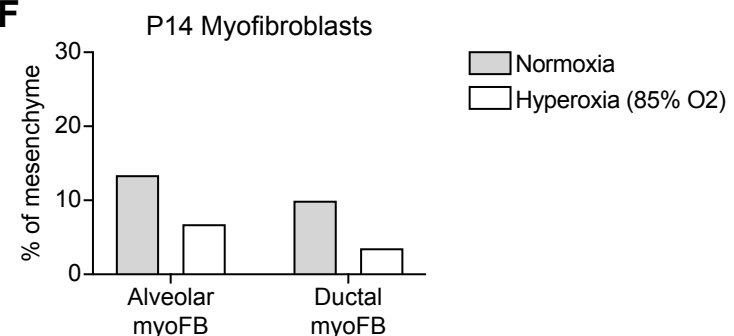
D Xia et al. Mesenchyme



E

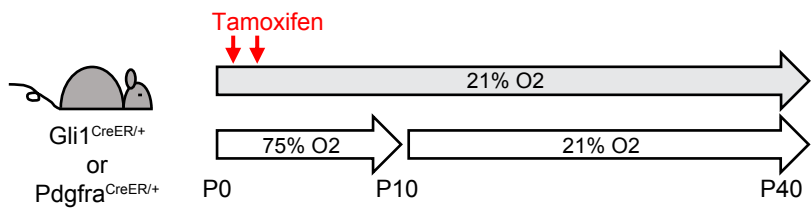


F

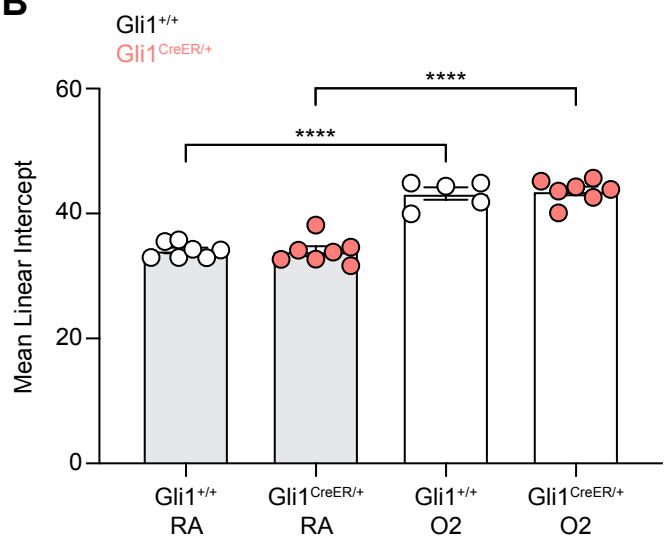


Supplementary Figure 3

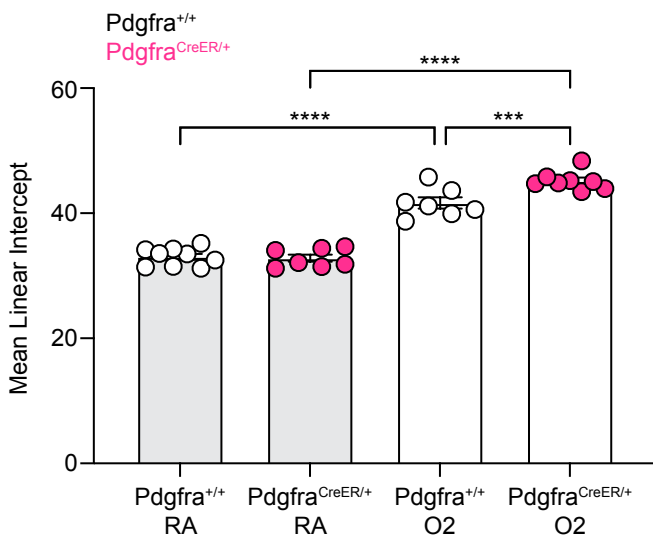
A



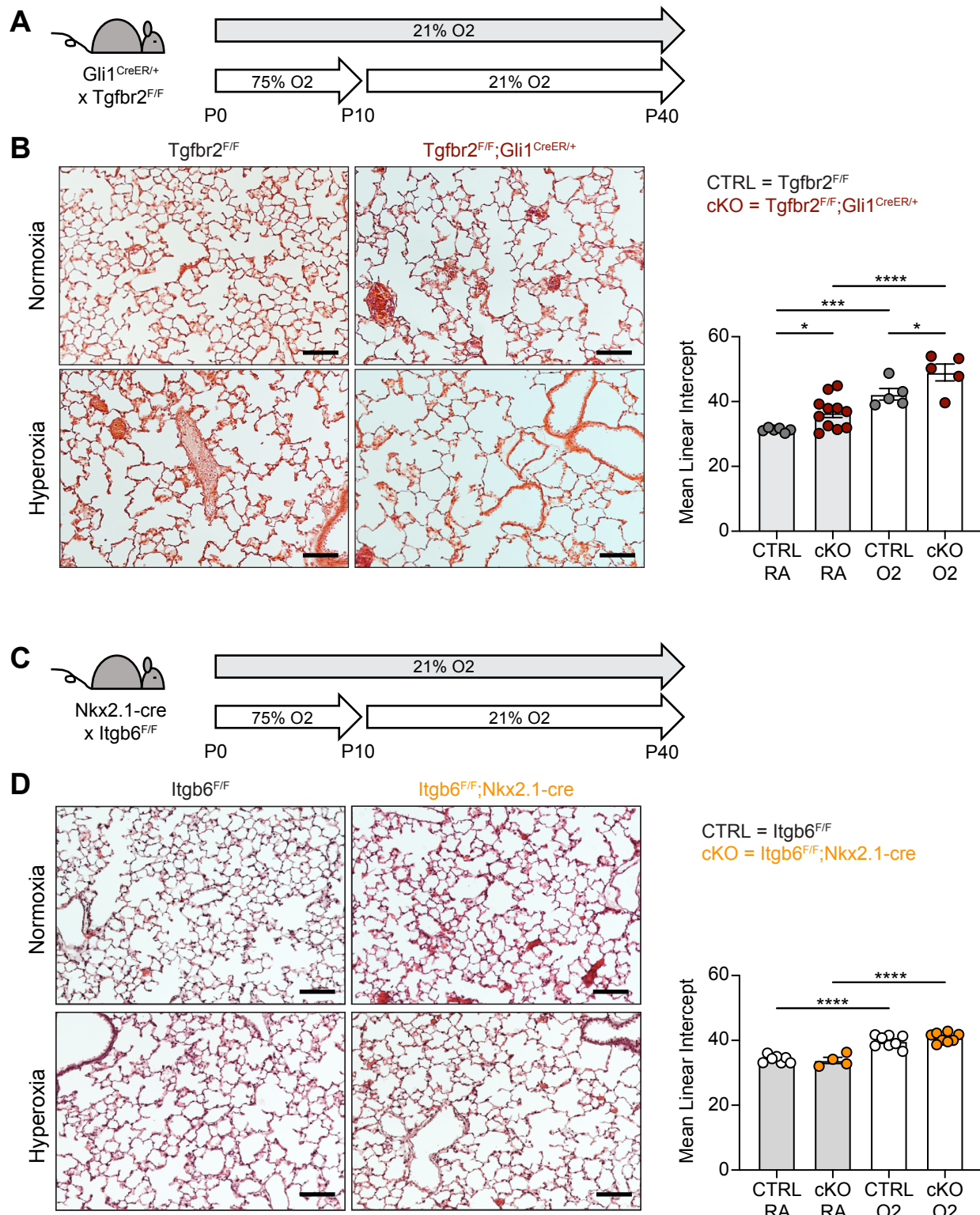
B



C



Supplementary Figure 4



Supplementary Figure 5

A

